

This is a pre-print of a manuscript submitted to Paleooceanography and Paleoclimatology and posted to EarthArXiv. It has not yet undergone peer review and will likely change before it is finalized. Comments are very welcome, and should be sent to the corresponding author (cmlowery@utexas.edu)

1 Seismic Stratigraphy of Contourite Drift Deposits Associated with the 2 Loop Current on the Eastern Campeche Bank, Gulf of Mexico

3 Christopher M. Lowery^{1*}, Ligia Perez Cruz^{2,3}, Jaime Urrutia Fucugauchi^{2,3}, Jingxuan Wei¹, James A.
4 Austin, Jr.¹, Patricia Standring¹

5 ¹Institute for Geophysics, Jackson School of Geosciences, University of Texas, Austin, USA

6 ²Instituto de Geofísica, Universidad Nacional Autónoma De México, Mexico City, Mexico

7 ³Instituto de Investigación y Estudios Avanzados Chicxulub, Merida, Yucatan, Mexico

8 *corresponding author: cmlowery@utexas.edu

9 10 **Key Points:**

- 11 • High resolution multichannel seismic data reveal the evolution of contourite drifts
12 associated with the Loop Current
- 13 • Contourite deposition began in the Cenozoic, and overlies early Cenozoic and Late
14 Cretaceous pelagic sediments with little evidence of bottom currents
- 15 • Comparison of seismic facies with those present at nearby Deep Sea Drilling Project Site 95
16 suggest the Loop Current began in the Early Oligocene

17 **Abstract**

18 The Loop Current is a key component of the northward transport of warm, salty water and
19 an important influence on Gulf of Mexico hydrography. Understanding how the Loop Current will
20 respond to ongoing anthropogenic warming is critically important, but the history of the Loop
21 Current is poorly known. Here, we present the results of a high resolution multichannel seismic
22 survey of sediment drifts on the eastern Campeche Bank associated with the Loop Current. We
23 identify three seismic megasequences: Megasequence A is an Early Cretaceous carbonate platform,
24 Megasequence B comprises Cretaceous to early Cenozoic pelagic carbonates with weak/no
25 contourite current flow, and Megasequence C comprises a series of large contourite drifts
26 representing the inception and history of the Loop Current. The base of the contourites is marked
27 by a regionally mappable unconformity eroding underling strata, sometimes incising hundreds of
28 meters. The drifts contain a succession of sequence sets separated from each other by regional
29 unconformities and comprising massive elongated mounded sediment drifts, then plastered drifts,
30 and then back the massive elongated drifts which characterize modern deposition, with active
31 moats forming on the seafloor. A lack of sediment cores in the study area precludes age
32 determination of these drift deposits, with the exception of the youngest (Late Pleistocene).
33 Comparison to legacy seismic lines across Deep Sea Drilling Project Site 95, just outside our study
34 area, implies that the base of Megasequence C is Oligocene, and that the Loop Current developed
35 during the global reorganization of ocean circulation at the Eocene-Oligocene Transition.

36 **Plain Language Summary**

37 The Loop Current flows into the Gulf of Mexico from the Caribbean through the Yucatán
38 Strait, and exits to the Atlantic Ocean through the Straits of Florida. The Loop Current is part of a
39 series of currents that carry warm, salty water to the far North Atlantic, where it cools and sinks, a
40 critical part of global ocean circulation. It is also important for Gulf of Mexico climate, as it
41 sometimes spins off warm eddies which drift west, disrupting fisheries and providing a warm
42 water fuel source for hurricanes. Because it is so important to global and regional climate, it is
43 important to understand how the Loop Current will respond to ongoing climate change, and one
44 essential part of that is seeing how it responded to past climate change. Here, we report the results

45 of a seismic survey of a sediment drift on the eastern Campeche Bank which records the initiation
46 and history of the Loop Current. A lack of sediment cores in this area make it hard to put age
47 constraints on our observations, so we evaluate several plausible hypotheses about when the Loop
48 Current first formed and what that means for the current's future.

49 **1. Introduction**

50 The Loop Current (Figure 1) is a key component of the global thermohaline circulation and
51 an important driver of regional and global climate. As one of the main feeder currents of the Gulf
52 Stream, the Loop Current is a major part of the western boundary current system in the North
53 Atlantic that moves warm, salty water from the tropics towards the Greenland, Iceland, and
54 Labrador seas, where it cools and sinks to form North Atlantic Deep Water, the main driver of
55 Atlantic Meridional Overturning Circulation (AMOC). The Loop Current also controls the average
56 oceanographic characteristics of surface waters in the Gulf of Mexico by aperiodically spinning off
57 warm-core eddies which drift west (Thirumalai et al., 2021). Eddy shedding is a complex process
58 that remains only partially understood (e.g., Weisberg and Liu, 2017). Individual eddies can
59 disrupt fisheries, strain offshore infrastructure, and provide a potent warm-water fuel source for
60 hurricanes (e.g., Biggs, 1992, Bosart et al., 1999; Milkov and Sassen, 2000). Warming attributed to
61 these eddies is also a possible driver of sea level rise rates in the Gulf of Mexico that exceed the
62 global average (Steinberg et al., 2023).

63 For these reasons, it is imperative to understand how the Loop Current will respond to
64 anthropogenic warming. The National Academies of Science, Engineering, and Medicine (NASEM)
65 recently published a detailed report cataloguing all the things that we do not know about the Loop
66 Current (NASEM 2019), emphasizing knowledge gaps regarding modern hydrography and eddy
67 formation. This publication was followed by the announcement of a NASEM funding program to
68 address these knowledge gaps using hydrographic observations and modelling. A glaring gap in
69 this important effort is the lack of any perspective on past Loop Current changes. Modern
70 hydrographic observations provide an important mechanistic understanding of the dynamic
71 processes which govern the Loop Current, but only within the narrow climatological framework of
72 the late 20th and early 21st centuries. As atmospheric $p\text{CO}_2$ approaches levels last reached in the

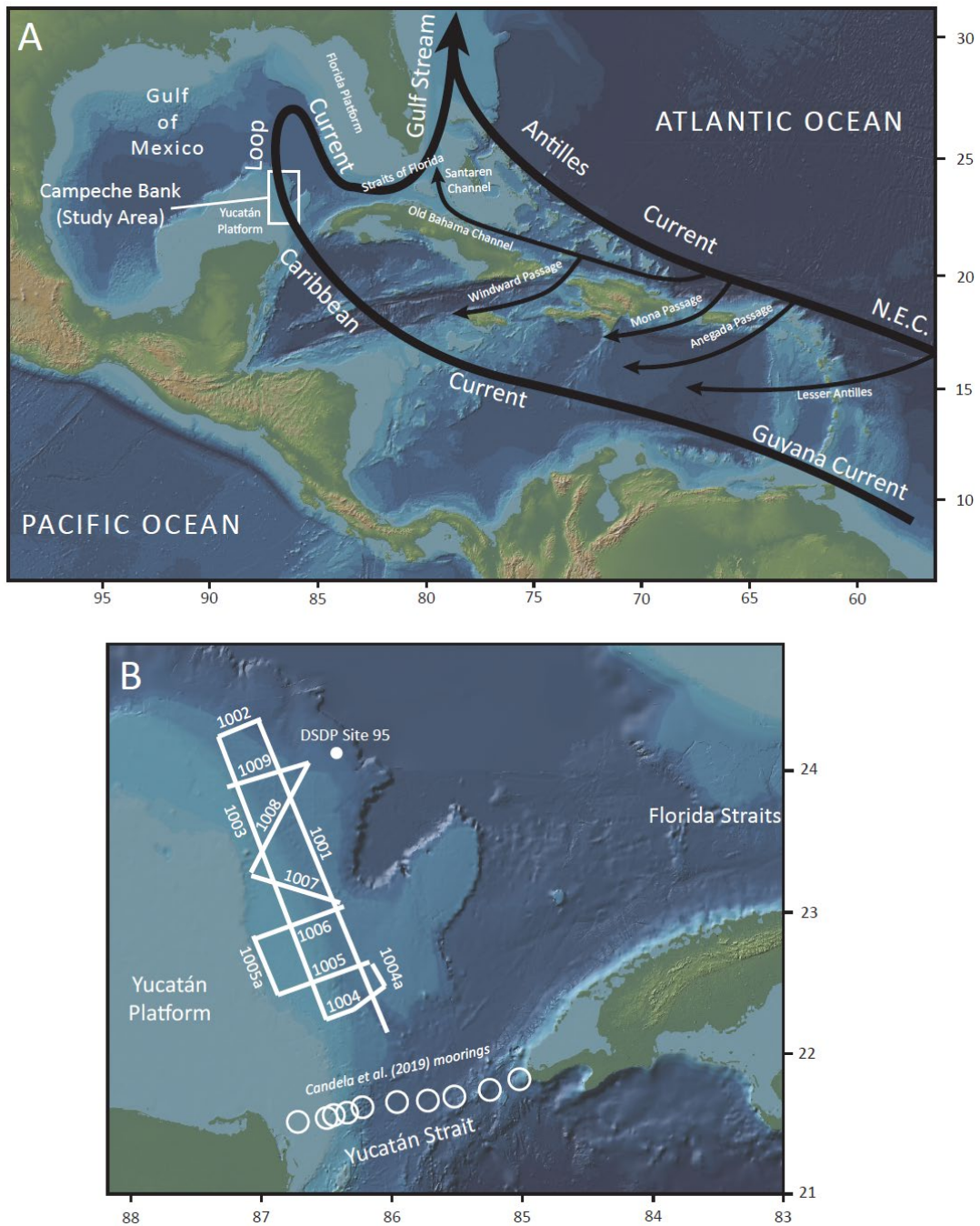


Figure 1. A) Regional surface currents associated with the North Atlantic western boundary current, including key oceanic gateways and passages for leakage of Northern Equatorial Current (N.E.C.) and Antilles Current waters into the Caribbean. B) Location map of the eastern Campeche Bank and surrounding waters, showing the location of our seismic survey, DSDP Site 95, and the mooring stations used to construct the vertical velocity profile reported in Candela et al. (2019) (Figure 2). Basemap is the Global Multi-Resolution Topography dataset (Ryan et al., 2009) plotted in GeoMapApp (www.geomapapp.org) / CC BY.

74 Miocene (e.g., Steinthorsdottir et al., 2021) with no sign yet of slowing down, we must understand
75 how the Loop Current operated during past analog climate states.

76 In particular, it is still unknown when the Loop Current first developed its modern
77 characteristics. How long has a current roughly the size and strength of the Loop Current been
78 established in the Gulf of Mexico? The general consensus is that the inception and subsequent
79 development of the Loop Current are closely tied to tectonic events in the Caribbean. Flow from
80 the Gulf of Mexico into the North Atlantic dates back to the Late Cretaceous (Chen, 1965; Pinet and
81 Popenoe, 1985), first through the Suwannee Straits cutting across northern Florida (also known as
82 the Gulf Trough; e.g., Popenoe et al., 1987), and then, by the Paleocene, through the Florida Straits
83 as well (Denny et al., 1994). The closure of the Suwannee Straits in the Oligocene is sometimes
84 cited as the cause of the inception of a (proto-) Loop Current that was weaker than the modern
85 Loop Current but, for the first time, was forced to make its namesake loop in the eastern Gulf to
86 exit through the Florida Straits (Gardulski et al., 1991; Hine, 2013).

87 This proto-Loop Current is generally agreed to have strengthened significantly in the
88 Middle Miocene around 14 Ma based on seismic stratigraphic architecture and cores from the
89 western Florida Platform, where the southward flowing arm interacts with the seafloor (Mullins et
90 al., 1987; Gardulski et al., 1991). This is coincident with the roughly simultaneous inception of
91 sediment drifts in the Florida Straits (Mullins and Neumann, 1979; Mullins et al., 1980; Denny et
92 al., 1994) and the Santaren Channel in the Bahamas (Anselmetti et al., 2000; Paulat et al., 2019).
93 The Santaren Channel sediment drifts are well dated by ODP cores to ~ 12.3 Ma (Paulat et al.,
94 2019). This Middle Miocene intensification is often cited as the start of the “modern” Loop Current
95 (e.g., Gardulski et al., 1991; Denny et al., 1994).

96 However, the driver for this Middle Miocene current intensification is unclear. Many older
97 studies associated it with the closure of the Central American Seaway (e.g., Mullins et al., 1987;
98 Gardulski et al., 1987; Denny et al., 1994; Roth et al., 2000), but improved dating and comparison
99 of deep-sea cores on either side of the Panamanian Isthmus have shown that closure of the Central
100 American Seaway postdates the Middle Miocene (see review by O’Dea et al., 2016). The closure of
101 the Central American Seaway proceeded in stages, with a closure of deep-water flow beginning in
102 the Late Miocene between 9.8 and 7.0 Ma and a final closure to surface flow with the formation of

103 the Isthmus of Panama in the mid Pliocene, around 2.8 Ma (O’Dea et al., 2016). Surface flow is the
104 important aspect of this closure for the Loop Current, as the flow of warm, salty Caribbean surface
105 water to the Pacific was blocked and redirected north where it flowed around Cuba into the Gulf of
106 Mexico through the Yucatán Strait to the west and through the Santaren Channel to the east. If the
107 closure of the Central American Seaway was the principal trigger for the formation of the Loop
108 Current, this implies that the Loop Current formed around the mid Pliocene.

109 Evidence for increased current flow in the mid Pliocene exists on both sides of Cuba.
110 Increased seafloor scouring (indicated by an increase in coarse fraction percentage in sediment
111 cores) has been observed in the Yucatán and Florida Straits in the mid Pliocene (Brunner, 1984).
112 On the western margin of Great Bahama Bank near the junction with the Florida Straits, a
113 significant mid Pliocene shift in current flow characterized by a major increase in erosion is
114 observed in drift deposits in Santaren Channel (Anselmetti et al., 2000). But these changes occur
115 within drifts which all date back to the Middle Miocene, and it seems that the closure of the
116 Central American Seaway likely only briefly invigorated an already strong current (Paulat et al.,
117 2019).

118 Other Caribbean gateway changes occur or are thought to occur in the Middle Miocene,
119 including the opening of ocean gateways in the Antilles, although these were always open to
120 surface flow (e.g., Pindell and Kennan, 2009), and the foundering of the Northern Nicaraguan Rise
121 carbonate “megabank” (e.g., Droxler, 1998; Roth et al., 2000; Mutti et al., 2005). The latter event
122 is proposed by Roth et al. (2000) to be the precipitating event in the inception of the Loop
123 Current, which according to this model was completely blocked by the presence of this large
124 shallow carbonate bank south of the Yucatán Strait. Calcareous nannofossil data from ODP Sites
125 998 and 999 show that nannofloras in the northern and southern Caribbean become more similar
126 starting 10.7 Ma, corroborating this idea (Kameo and Sato, 2000). However, evidence for deep
127 water flow out of the Gulf of Mexico extends back to the Eocene (e.g., Denny et al., 1994) suggests
128 this bank was not an impairment to flow from the Caribbean to the Gulf, and in any case this
129 hypothesis cannot account for the Middle Miocene development of sediment drifts in the Bahamas
130 (e.g., Anselmetti et al., 2000), which would have been unaffected by the Nicaragua Rise

131 “megabank.” All in all, a tectonic trigger for the inception of the Loop Current is not supported by
132 current data.

133 The Middle Miocene is also associated with progressive cooling of the Miocene Climate
134 Transition (e.g., Holbourn et al., 2022), coeval with the inception of the modern Antarctic
135 Circumpolar Current (Livermore et al., 2007) and strengthening North Atlantic Deep Water
136 formation driving abyssal contourite development in the western North Atlantic (Knutz et al.,
137 2008; Boyle et al., 2017). These examples of current strengthening all point to an overall
138 invigoration of Atlantic Meridional Overturning Circulation (AMOC) of which the Loop Current is
139 a key part. This would indicate that the initiation of the Loop Current was triggered by climate
140 change in some earlier warm state. If this is the case, it means that a modern climate change back
141 toward that earlier warm state could cause the Loop Current to weaken and, perhaps, cross a
142 tipping point resulting in a fundamental change ocean circulation.

143 In order to identify such a tipping point, we must better constrain when the Loop Current
144 first developed. The Campeche Bank, just north of the Yucatán Channel where the Loop Current
145 first enters the Gulf of Mexico, is perhaps the best place to investigate the history of the Loop
146 Current, because it records the full history of flow into the Gulf of Mexico. Other sedimentary
147 archives of Loop Current flow on the western Florida Shelf are biased by variations in the
148 maximum northern extent of the loop, and proxy records from that location and the Florida
149 Straits are biased by Mississippi River outflow, whose cool fresh water dilutes the signal of warm
150 salty Caribbean water. The eastern Campeche Bank is the only place where a pristine record of the
151 Loop Current, as it first enters the Gulf, can be investigated.

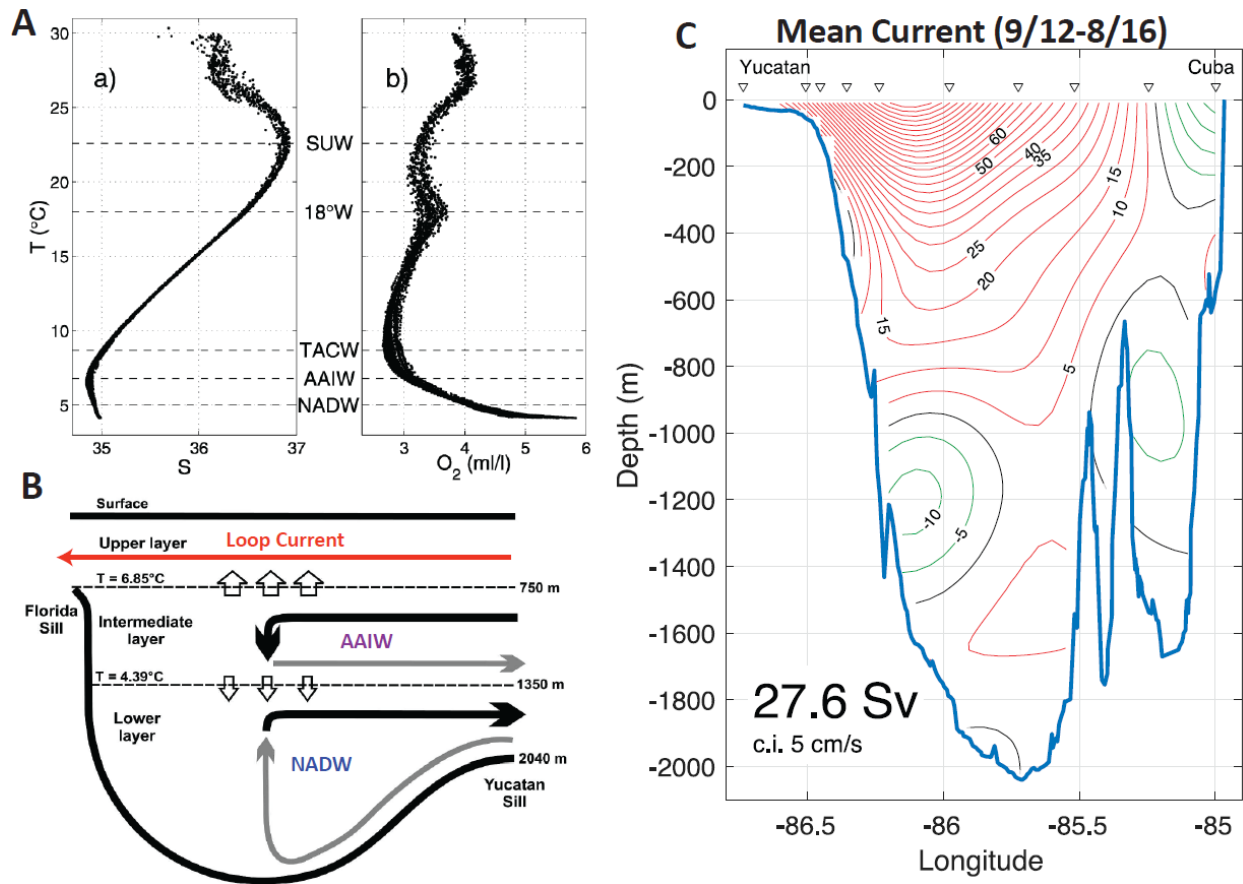
152 The presence of an active sediment drift on the Campeche Bank has been known for years
153 thanks to the pioneering work of Hübscher and colleagues on successive cruises of the *R/V Meteor*
154 (Hübscher et al., 2010; Hübscher and Nürnberg, 2023; Hübscher et al., 2023). To reconstruct the
155 history of this drift we carried out a multichannel seismic survey on the *R/V Justo Sierra* in July
156 2022 (Figure 1B). Resultant high resolution seismic profiles allow us to understand the
157 stratigraphy of these deposits and constrain the timing of their formation. Although the paucity of
158 sediment cores in this area makes age control tenuous, our data strongly suggest that the Loop

159 Current predates the closure of the Central American Seaway and may date back to the Eocene-
160 Oligocene Transition.

161 **2. The Loop Current**

162 The Loop Current dominates surface circulation in the Gulf of Mexico, which it enters
163 through the Yucatán Strait and exits through the Florida Straits (Figure 1). Rather than tracing a
164 direct path between these two gateways, the Loop Current first flows northward into the Gulf
165 before swinging back south, forming the loop from which it gets its name. The northward extent
166 of this loop varies as the result of wind patterns and the position of the intertropical convergence
167 zone (ITCZ; Poore et al., 2004; Arrellano-Torres and Amezcua Montiel, 2022). Aperiodically (every
168 6-11 months), this loop pinches off and forms a warm-core anticyclonic eddy that drifts west
169 across the Gulf (e.g., Sturges and Leben, 2000; Candela et al., 2002). These eddies are associated
170 with a number of hazards, including a drop in surface water productivity (Biggs, 1992), altered
171 larval fish dispersion (Lindo-Atichati et al., 2012), reduced stability of shallow gas hydrates
172 (Milkov and Sassen, 2000), and rapid intensification of tropical cyclones (e.g., Bosart et al., 1999;
173 Jaimes et al., 2016), notably including hurricanes Katrina (Jaimes and Shay, 2009) and Harvey
174 (Potter et al., 2019). Eddies also drive vertical mixing of deep and surface water masses in the Gulf
175 (Welsh and Inoue, 2000). Both eddy formation and Yucatán inflow (i.e., transport of Caribbean
176 water through the Yucatán Channel into the Loop Current) vary seasonally, with Yucatán inflow
177 stronger in the summer (e.g., Candela et al., 2002; Rousset and Beal, 2011) and eddy formation
178 more common in the winter (Chang and Oey, 2012). Loop Current flow and the position of the
179 loop are also strongly influenced by eddy formation in the northwestern Caribbean (Androulidakis
180 et al., 2021).

181 The Loop Current is driven by a combination of wind stress and meridional overturning
182 circulation (Schmitz and McCartney, 1993). The water transported through the Gulf of Mexico by
183 the Loop Current is characterized by Caribbean water masses, summarized by Rivas (2005) and in
184 Figure 2. Below the surface the Loop Current is characterized by warm, salty Subtropical
185 Underwater (SUW) which forms in the northern and southern subtropics where high evaporation
186 predominates (Rivas et al., 2005). SUW is overlain by a slightly fresher surface water mass diluted



187

Figure 2. Southeastern Gulf of Mexico hydrography. A) Temperature (T)/Salinity (S) and Temperature/Oxygen (O_2) for Yucatán Channel from Rivas et al. (2005) showing the watermasses that enter the Gulf through this aperture; SUW: Subtropical Underwater; $18^\circ W$: $18^\circ C$ Sargasso Sea Water; TACW: Tropical Atlantic Central Water; AAIW: Antarctic Intermediate Water; NADW: North Atlantic Deep Water. B) Generalized schematic of circulation through the Gulf of Mexico, modified from Rivas et al. (2005). C) Mean current velocity in cm/s through the Yucatán Channel from September 2012 to August 2016 slightly modified from Candela et al. (2019). Red contours represent northward flow and green contours southward counterflow; see Figure 1 for mooring locations.

188

189 by Amazon outflow and Caribbean precipitation (Rivas et al., 2005). Below SUW, $18^\circ C$ Sargasso
 190 Seawater, characterized by an oxygen maximum, and Tropical Atlantic Central Water (TACW),
 191 characterized by an oxygen minimum, round out the upper water column down to ~ 700 m water
 192 depth (Rivas et al., 2005). The Florida and Yucatán Straits have different sill depths, with the
 193 Florida sill (~ 750 m) shallower than the Yucatán (~ 2040 m). Northward transport through the
 194 Gulf of Mexico via the Yucatán Channel and the Florida Straits is thus limited to the upper 750 m

195 (Rivas et al., 2005). The Yucatán Channel is the only pathway for deep water masses to enter the
196 Gulf, which is filled by North Atlantic Deep Water (NADW) below a depth of roughly 1000 m and
197 Antarctic Intermediate Water between 1000 m and 700 m depth (Rivas et al., 2005).

198 As the Loop Current enters the Gulf of Mexico through the Yucatán Channel, its “core” is
199 50-100 km wide, and it has a mean velocity of 1.5 m/s (with a maximum of 2.5 m/s) (Abscal et al.,
200 2003; Ochoa et al., 2003; Badan et al., 2005; Candela et al., 2003, 2019). Moorings deployed
201 across the Yucatán Channel by Candela et al. (2019) show that current velocity decreases as a
202 function of depth, and the Loop Current interacts with the seafloor down to a depth of ~800 m
203 (Figure 2) (Candela et al., 2019). A southward flowing counter current impinges the seafloor on
204 the western side of the Yucatán Channel between roughly 1000 and 1400 m water depth (Candela
205 et al., 2019). Mean flow into the Gulf of Mexico is 27.6 Sverdrups (Candela et al., 2019).

206 **3. Methods**

207 **3.1 Data collection**

208 Seismic data were collected aboard the R/V *Justo Sierra* July 15-26, 2022. This cruise was
209 originally planned for the summer of 2020, but was twice delayed due to the pandemic. We used
210 the Scripps Institution of Oceanography portable multichannel seismic system, which consists of
211 two 75/75 cubic inch generator-injector (GI) air guns, a 750 m active-length Geo Eel streamer
212 with 120 channels of 4 hydrophones each spaced at 6.25 m, and four birds for depth control. The
213 air guns were rigged to fire in a 45 cubic inch configuration to allow an increased shot rate for
214 higher resolution, and were towed at a depth of 3 m. In order to maintain a roughly constant
215 speed over ground through and across the Loop Current we had to adjust our speed through the
216 water depending on the direction we were moving; shot rate was similarly adjusted to maintain
217 12.5 m shot spacing, creating a common midpoint (CMP) spacing of 3.125 m. For each shot, 4 s of
218 data were recorded at a sample rate of 0.5 ms and later resampled to 1 ms. A 50-ms layback was
219 created during each shot due to the distance-based recording system, which was later corrected
220 during data processing.

221 Our survey produced nine primary seismic profiles, labeled Lines 1001-1009 (Figure 1B).
222 These comprise two long strike lines and seven dip lines (two of which are not perpendicular to
223 strike due to time constraints). Additional profiles were collected along short lines connecting the
224 ends of the main profiles. Dip lines are roughly 20 km apart and do not extend all the way to the
225 distal edge of the Campeche Bank (a large submarine cliff called the Campeche Escarpment)
226 because that feature lies within the Cuban exclusive economic zone (EEZ). However, our survey
227 encompasses the large majority of the Campeche Bank drift deposits.

228 **3.2 Data processing**

229 We processed the data using the Paradigm application Echos with an emphasis of
230 preserving the high-resolution nature of the survey. The processing workflow began with data
231 importation and geometry definition. Extremely rarely during the acquisition, navigation was lost
232 due to system glitches. The missing shot navigations are calculated using linear interpolation
233 between existing coordinate locations. To enhance reflection amplitudes and reduce noise
234 contamination, we applied source wavelet deconvolution using Burg's method (Burg, 1975),
235 multichannel predictive deconvolution, a 40-320 Hz bandpass filter, trace editing, and spherical
236 divergence correction. Bad traces were removed during trace editing. We performed velocity
237 analysis interactively after sorting data into common mid-point (CMP) gathers; velocity functions
238 were picked every 100 CMPs (312.5 m) to flatten coherent reflections. Additionally, we drew mutes
239 to remove water column energy and far-offset stretching. After stacking, we used Kirchhoff post-
240 stack time migration to collapse diffractions and restore dipping reflections to their correct
241 positions (Yilmaz, 2001). Finally, we implemented depth conversion guided by depth-converted
242 velocity functions.

243 **3.3 Grain Size Analysis**

244 To test whether there is sedimentological evidence for a change in current velocity across
245 the Eocene-Oligocene Transition at Deep Sea Drilling Project (DSDP) Site 95 (for reasons
246 discussed in detail below) we requested samples from Cores 2-8 (Lower Oligocene through middle
247 Eocene; Worzel et al., 1971). These samples were soaked overnight in DI water and then run

248 through a Mastersizer 3000 laser grain size analyzer and output at quarter-phi steps. The 10-63
249 μm size fraction was then plotted stratigraphically to track changes in “sortable silt,” a common
250 proxy for bottom water current flow (e.g., McCave et al., 2017).

251 **3.4 Data interpretation**

252 Processed and depth-converted seismic profiles were interpreted using the Echos
253 interpretation program for the Paradigm software package.

254 Ocean currents moving across the seafloor can build extensive accumulations of
255 sediments, known as contourite drifts, so-called because they typically develop parallel or slightly
256 oblique to continental margins, and thus follow contour lines, in contrast with down-slope
257 currents like turbidites (Rebesco et al., 2014). As the sedimentological expressions of ocean
258 currents, contourite deposits are exceptional archives of ocean circulation and climate history, and
259 are typically the target of extensive sampling campaigns to understand their geometries and
260 physical characteristics. In particular, high-quality seismic data have allowed detailed
261 morphological categorization of contourite drifts (see review by Rebesco et al., 2014). Contourite
262 drifts have unique internal geometries that are mappable at a seismic scale and distinguishable
263 from stratigraphically adjacent non-contourite deposits (Faugères et al., 1999; Nielsen et al., 2008;
264 Rebesco et al., 2014; Boyle et al., 2017). In particular, sediment drifts tend to be bounded by
265 erosional discontinuities that are chronostratigraphically synchronous, can be traced across the
266 entire drift, and are typically associated with a shift in seismic facies corresponding to a shift in
267 current strength (e.g., Faugères et al., 1999; Rebesco et al., 2014). Horizontal or low angle dipping
268 reflectors truncated at the seafloor or by an internal discontinuity are also common features of all
269 sediment drifts (Faugères et al., 1999; Rebesco et al., 2014). We used these criteria to identify and
270 differentiate contourite drifts in our seismic profiles.

271 We mapped three seismic megasequences (megasequences A, B, and C) defined by unique
272 internal characteristics and separated from each other by distinct seismic horizons that are
273 mappable across the entire study area. Megasequences B and C were then subdivided into
274 sequence sets based on the occurrence of internal horizons marking seismic facies change within

275 the megasequence (Figure 3). Seismic interpretation follows previous work in the Gulf of Mexico,
276 including Buffler et al. (1980), Angstadt et al. (1985), Denny et al. (1994), Marton and Buffler
277 (1999), Sanford et al. (2016), Snedden and Galloway (2019), and Sickmann and Snedden (2020).

278 The only age control in our study area comes from an 11.4-m piston core collected by the
279 R/V *Meteor* and dated to the Late Pleistocene by Hübscher and Nürnberg (2023). DSDP Site 95 sits
280 a few kilometers downdip of our study area at the toe of the Campeche Bank drifts within the
281 Cuban EEZ (and thus was not included in our survey). The Cretaceous-Paleogene (K/Pg) boundary
282 deposit forms a bright, easily mappable reflector across the Gulf of Mexico (e.g., Buffler et al.,
283 1980; Denne et al., 2013; Sanford et al., 2016); this event layer is also present on the eastern
284 Campeche Bank and provides a useful marker to constrain the ages of the overlying sediments.
285 Between this reflector and the Pleistocene core collected by Hübscher and Nürnberg (2023), we
286 are only able to determine relative ages of the seismic units described below. Making some
287 reasonable assumptions based on context and nearby cores, we then discuss what we interpret to
288 be the most likely ages of these units.

289 **4. Results**

290 We interpret three seismic megasequences, corresponding to acoustic basement (MSA);
291 relatively flat-lying, high amplitude reflectors (MSB); and dipping, downlapping, low amplitude
292 reflectors separated from MSB by an erosive disconformity (MSC). MSB and MSC are subdivided
293 into sequence sets on the basis internal facies changes and disconformities. These seismic units,
294 their bounding horizons, internal facies, interpreted depositional environment, and age (if known)
295 are summarized in Figure 3. Each megasequence is described in detail below. Key profiles are
296 illustrated in Figures 4-9. Larger, higher-resolution interpreted and uninterpreted seismic profiles
297 are included as supplemental material.

298 **4.1 Megasequence A**

299 Megasequence A (MSA) is the deepest seismic unit observed and therefore represents
300 acoustic basement. Snedden and Galloway (2019) map Albian and older platform carbonates

301 across the Yucatán Platform and around much of the Gulf rim; we interpret our MSA as
302 corresponding to these carbonates. MSA is bounded at the top by seismic horizon H1. Reflectors of

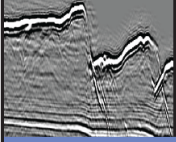
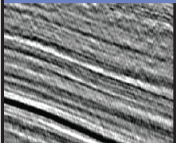
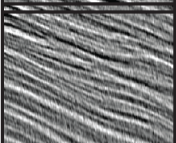
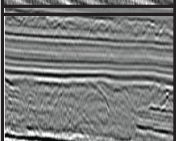
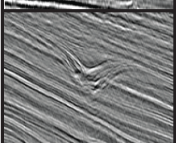
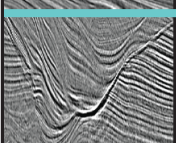
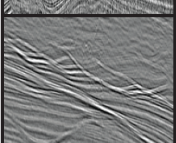
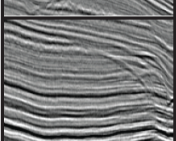
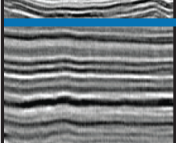
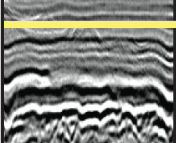
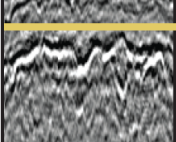
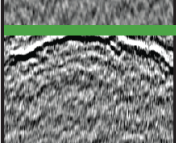
Seismic Facies	Seismic Facies Description	Seismic Facies Interpretation	Seismic Sequence	Age	Horizon
	High amplitude continuous reflectors draped across a basal unconformity eroding underlying units	Active mounded contourite drifts	MSC 3	Recent-mid Pleistocene (1 Ma) (Hübscher and Nurnberg, 2023)	H6
	Medium to high amplitude continuous, dipping reflectors downlapping on to underlying units	Plastered sediment drift with isolated small channel features, some sediment waves, and occasional mass transport complexes. Reflectors typically downlap onto MSC1, and are truncated at the seafloor.	MSC 2	Unknown	H5
	Medium to high amplitude wavy, crossbedded reflectors				
	Low amplitude, chaotic reflectors sometimes eroding underlying surfaces				
	medium to high amplitude small channel features with basal erosional surface				
	large cut and fill channels with medium to high amplitude reflectors, downlapping overbank deposits	Migrating contourite channel levee complexes. Erosive contact with underlying MSB.	MSC 1	Unknown	H4
	Medium to high amplitude wavy, crossbedded reflectors and amalgamated channels				
	Medium to high amplitude continuous reflectors downlapping on to underlying units				
	High amplitude, continuous, parallel reflectors	Interbedded pelagic sediments, possibly chert-bearing	MSB 3	Paleogene?	H3
	Very high amplitude incising reflectors, peak-trough-peak pattern	Mass wasting deposit associated with Chicxulub Impact	MSB 2	K/Pg boundary unit (Buffler et al., 1984; Angstadt et al., 1985; Denne et al., 2013, Sanford et al., 2016)	H2
	Low to medium amplitude, discontinuous reflectors	Pelagic chalk	MSB 1	Late Cretaceous (Santonian-Campanian) (Worzel et al., 1971)	H1
	Low amplitude chaotic reflectors	Platform carbonates, acoustic basement	MSA	Early Cretaceous (Albian and older) (Worzel et al., 1971)	H1

Figure 3. Seismic facies, seismic units, and key horizons identified in our seismic survey. See text for description of seismic megasequences and sequence sets. Figure design inspired by Boyle et al. (2017).

304

305

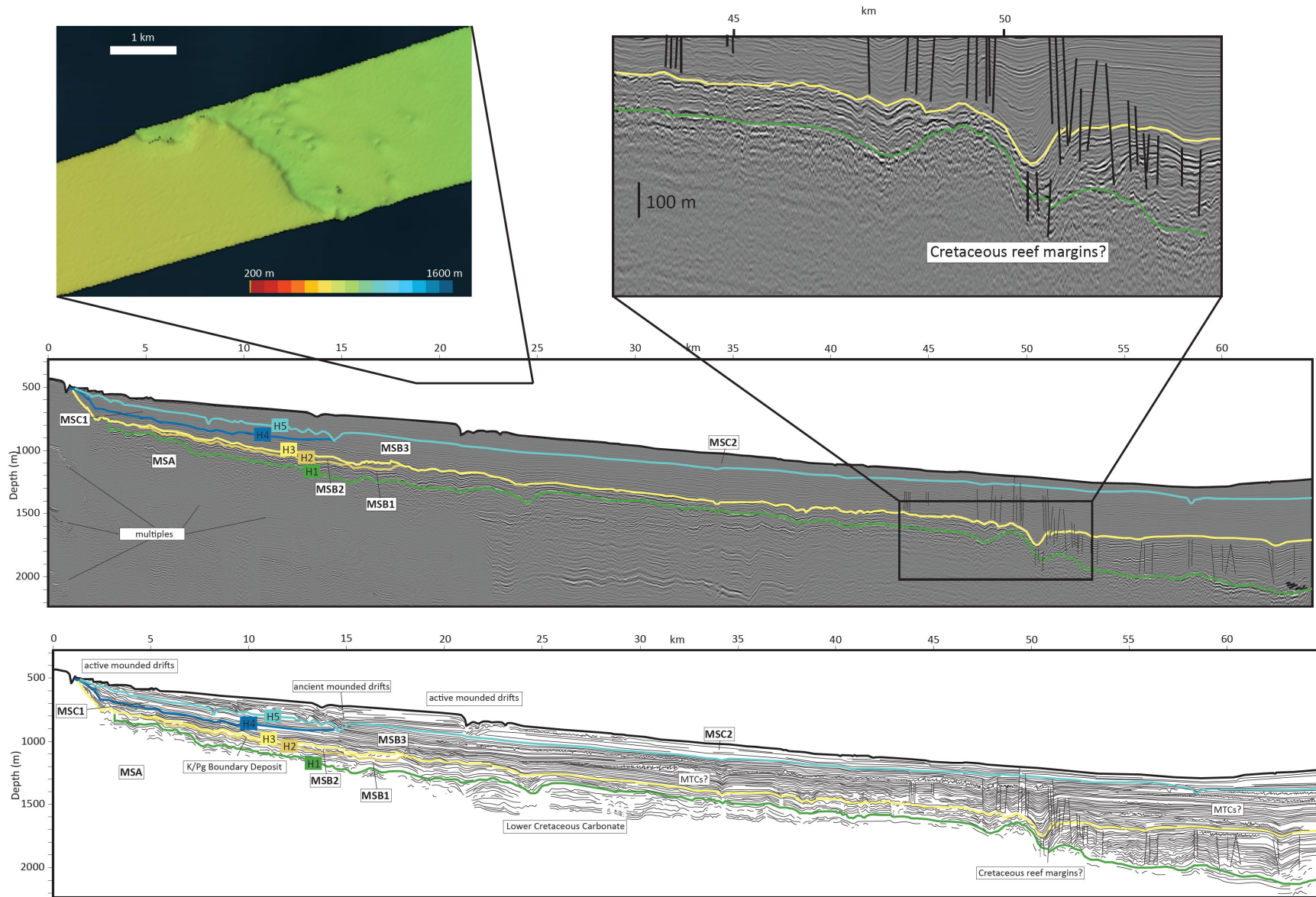


Figure 4. Interpreted seismic profile of Line 1009, on the northern end of our study area. This profile shows relatively thinner drift deposits of MSC2, while MSC1 is limited to just the most up dip area, and MSC3 is not identified. A) multibeam bathymetry of active contourite moat in western end of profile; B) inset interpreted seismic profile showing development of reef margins in MSA (note thickening of Cretaceous pelagic sediments down dip of these margins); C) interpreted seismic profile; D) line drawing of interpreted profile. See location map in Figure 1B.

307

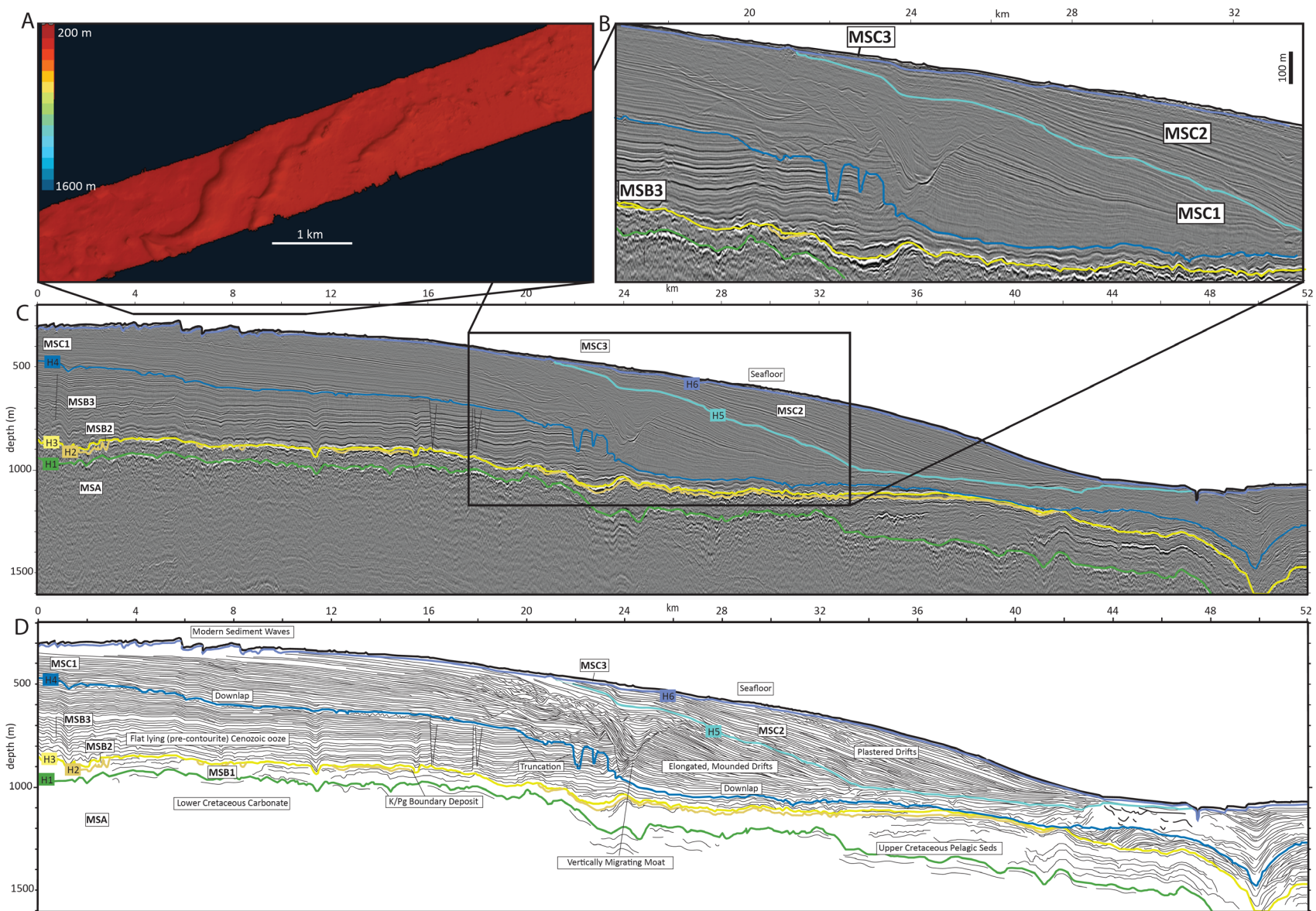
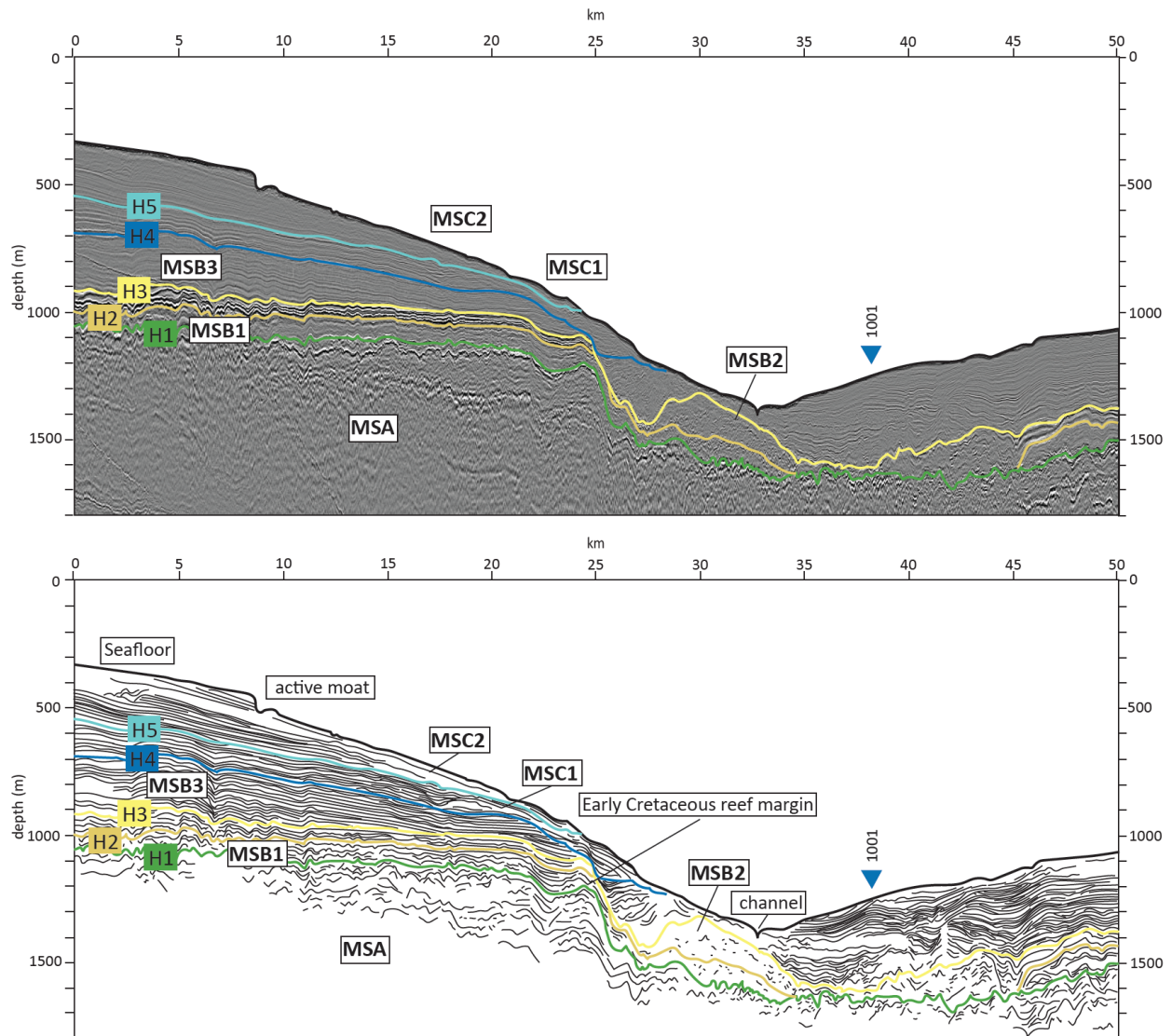


Figure 5. Interpreted seismic profile of Line 1005, which is notable for the dramatic incision of MSC1 into MSB, and for the large amalgamated channels in MSC1. (see inset). A) multibeam sonar bathymetry of sediment waves near western end of profile; B) inset interpreted seismic profile of notable erosional features in MSC1; C) interpreted seismic profile; D) line drawing of interpreted profile. See location map in Figure 1B.

309



310

Figure 6. Interpreted seismic profile of Line 1004, on the far southern end of our study area. The Campeche Bank drift is narrower here and mostly limited to the far western area of this profile, updip of a steep early Cretaceous reef margin. Note thick K/Pg mass transport deposit at the foot of this relict escarpment. A deeper water drift complex, unrelated to the Loop Current, can be seen on the eastern end of this profile. A) interpreted seismic profile; B) line drawing of interpreted profile. See location map in Figure 1B.

311

312

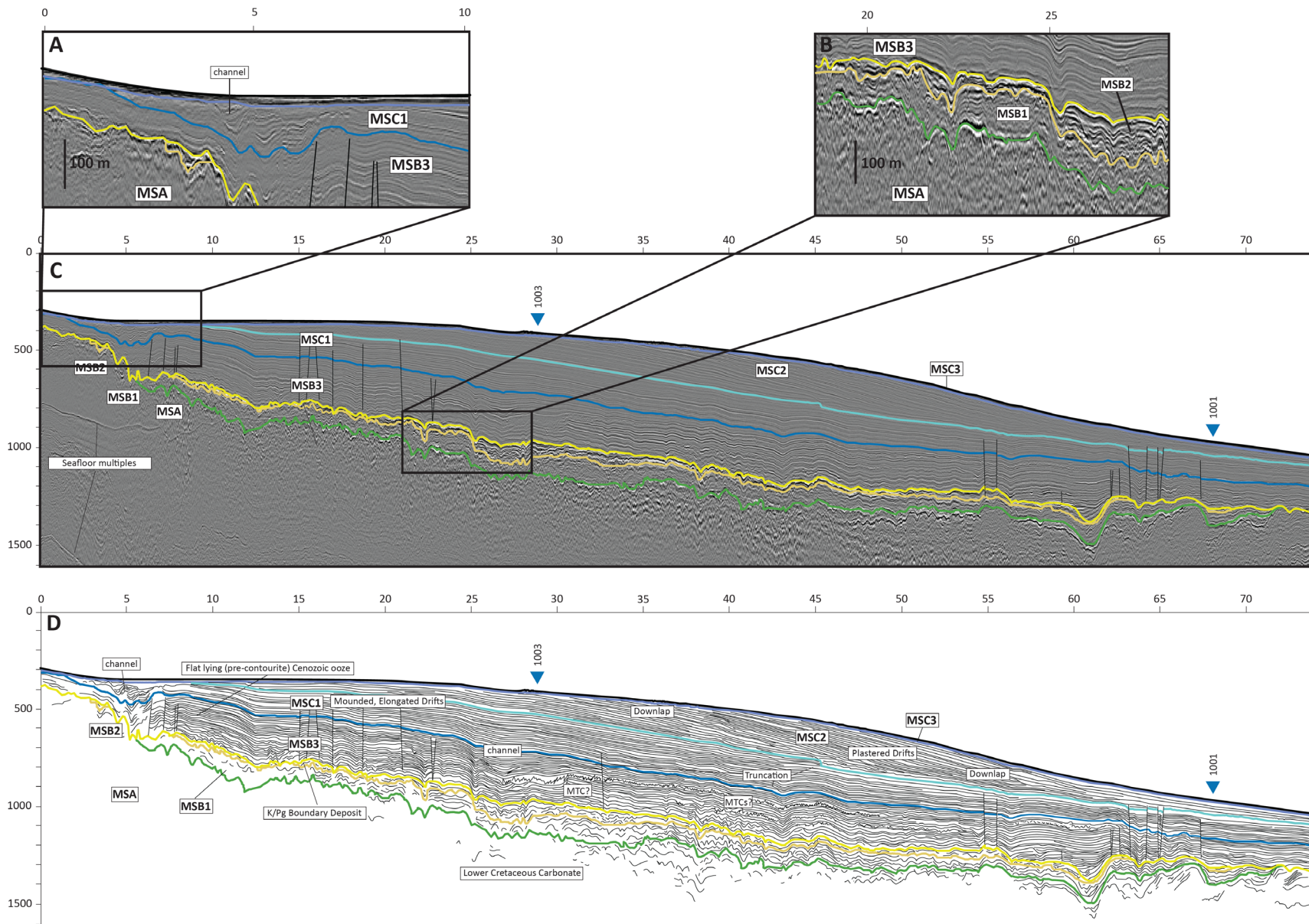
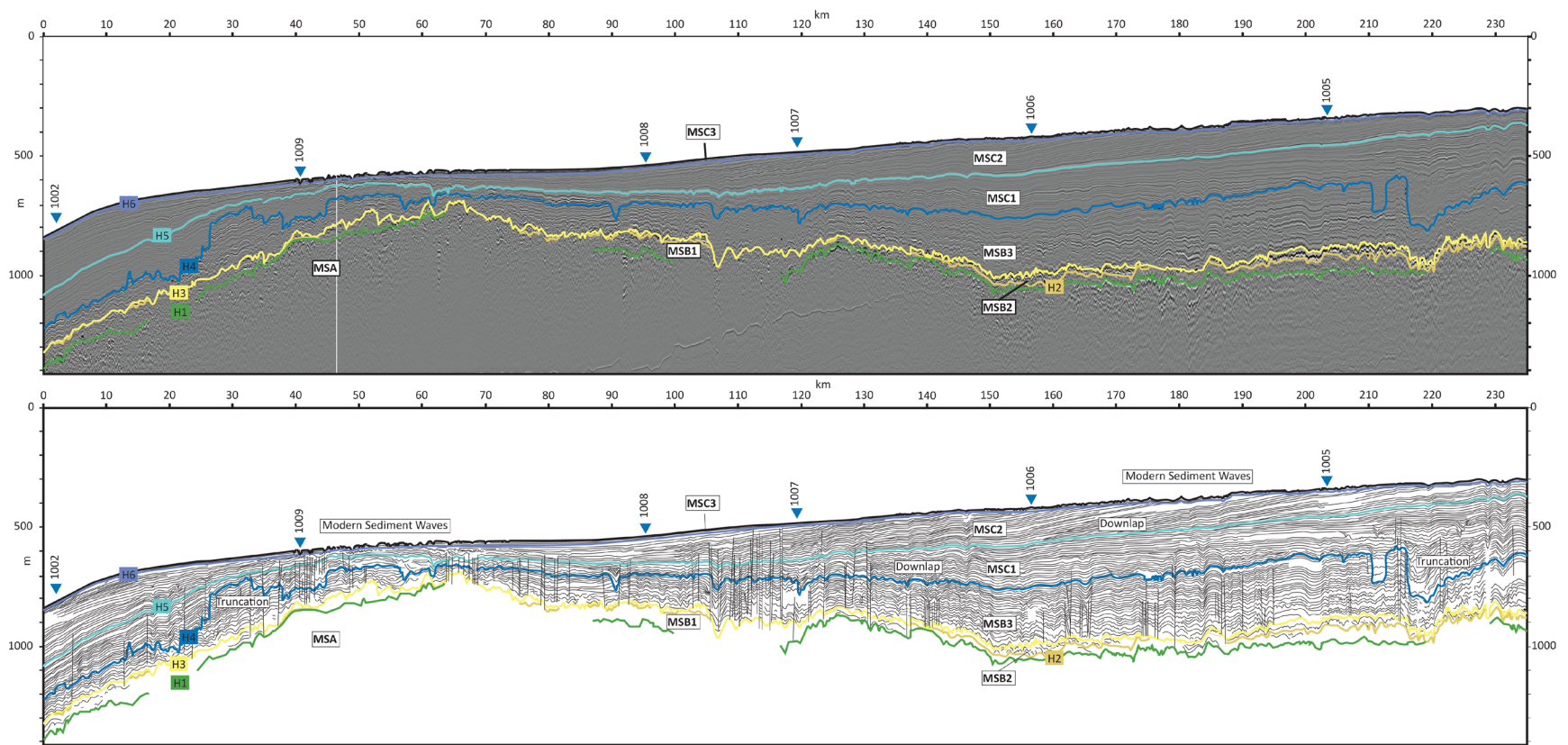


Figure 7. Interpreted seismic profile of Line 1006, in the central part of our study area. The Campeche Bank drift is thick but contains fewer channels than nearby Line 1005. A) An amalgamated channel complex is present at the far updip end of MSC1; B) characteristic K/Pg boundary deposit with thicker deposit with fairly thick (~100 m) build up in a paleo low; C) interpreted seismic profile; D) line drawing of interpreted seismic profile. See location map in Figure 1B.

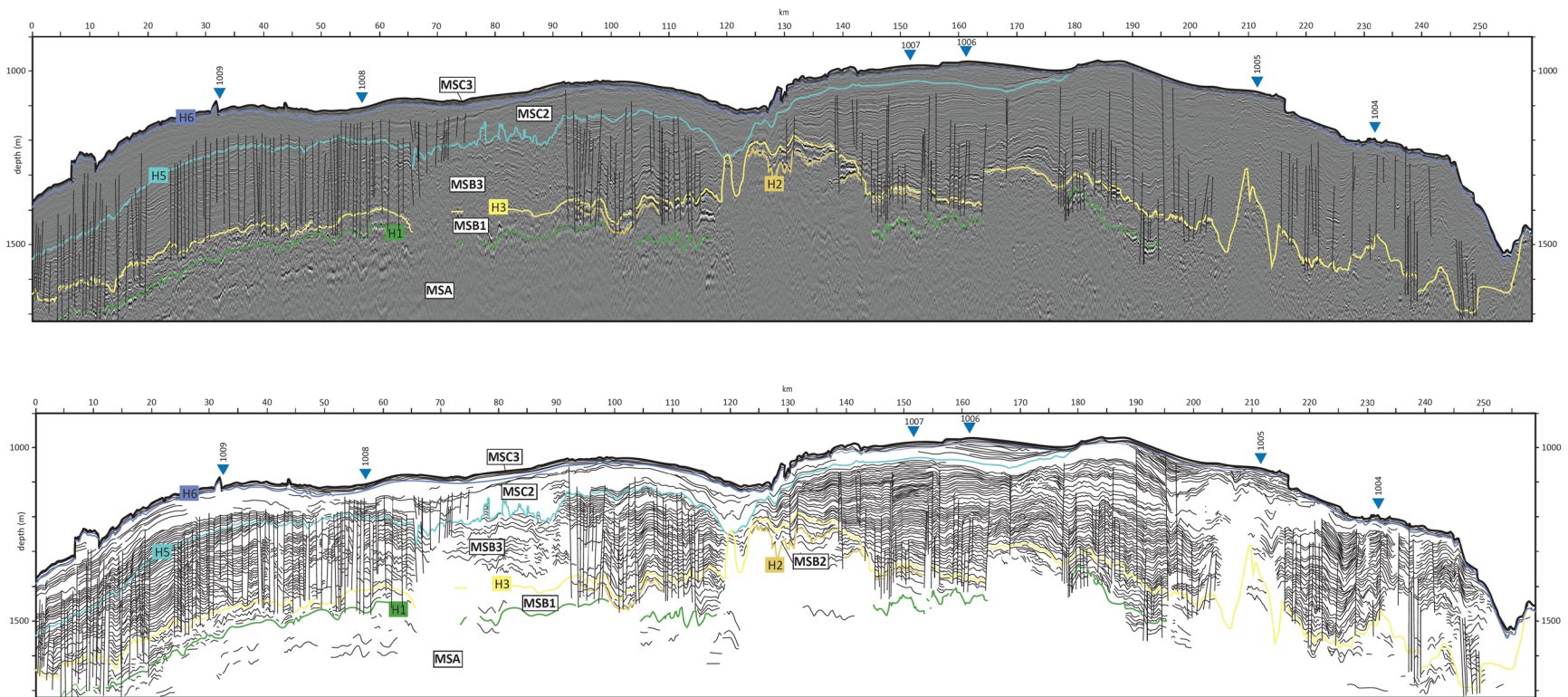
314



315

Figure 8. Interpreted seismic profile of Line 1003, the updip strike line. Northward dipping reflectors downlapping on Horizon H5 show deposition across the entire length of the contourite drift. Extensive erosion along Horizon H4 (representing the base of contourite drift deposition) occurs across the entire profile and is particularly evident at the far northern (left) and southern (right) ends. A) interpreted seismic profile; B) line drawing of interpreted seismic profile. See location map in Figure 1B.

316



317

Figure 9. Interpreted seismic profile of Line 1001, the downdip strike line. Of particular interest in this line is the erosional escarpment on the southern (right) end, facing the Campeche Channel. Even below 1000 m there appears to be active erosion at the seafloor. A) interpreted seismic profile; B) line drawing of interpreted seismic profile. See location map in Figure 1B.

318

319 the overlying MSB1 onlap and, in places, downlap on this horizon. MSA is characterized by low
320 amplitude, chaotic reflectors. In some places, mounded geometries are present within the unit
321 (Figure 3); these mounded geometries are often associated with a corresponding mound in
322 horizon H1, along with an increase in slope in the downdip direction. These features are best
323 developed in Line 1009 (Figure 4), and we interpret them to represent reef margins.

324 No core penetrations of MSA exist within our study area. At nearby DSDP Site 95, drilling
325 recovered Early Cretaceous (Albian and older) dolomitized carbonates from an ancient shallow
326 water carbonate platform which drowned as the basin subsided and sea level rose in the mid
327 Cretaceous (e.g., Buffler et al., 1980). This age and depositional environment agrees with the
328 regional interpretations of Snedden and Galloway (2019). The flat-lying, high amplitude reflectors
329 observed in the deepest part of MSA along Line 1009 (Figure 4) may represent anhydrite deposits,
330 which are known from the Aptian of both the Yucatán and Florida platforms, as well as the
331 Bahamas (Austin et al., 1986; Ward et al., 1995; Snedden and Galloway, 2019).

332 **4.2 Megasequence B**

333 Megasequence B (MSB) is comprised of parallel reflectors (sometimes subparallel, due to
334 interpreted faulting and folding) (Figure 3). These reflectors onlap onto seismic horizon H1, which
335 separates MSB from MSA. The upper contact with the overlying MSC is defined by seismic horizon
336 H4; this contact is characterized by an erosional unconformity across most of the study area. In
337 some places roughly parallel reflectors above and below H4 give it the appearance of a
338 paraconformity. In other places (best developed in Line 1005; Figure 5) this horizon H4 is
339 characterized by obvious erosion and incision, sometimes of more than 100 m. The parallel
340 reflectors of MSB are interpreted to indicate Late Cretaceous to Cenozoic pelagic sedimentation
341 without any evidence of contourite deposition. These pelagic sediments are divided by the K/Pg
342 boundary deposit, a layer of erosion and mass wasting 10s to 100s of m thick bounded by seismic
343 horizons H2 and H3. This bright, easily mappable event deposit splits MSB into three interpreted
344 sequence sets: MSB1 (Cretaceous pelagic sediments), MSB2 (K/Pg boundary deposit), and MSB3
345 (early Cenozoic pelagic sediments).

346 **4.2.1 Megasequence B1**

347 Megasequence B1 sits unconformably on top of the interpreted relict carbonate platform
348 and reef margins of MSA. Onlapping reflectors are evident at different positions along this contact
349 (particularly along lines 1005 and 1009). This unit gets progressively thicker down dip, and older
350 MSB1 reflectors exist down dip of relict reef margins of MSA, possibly indicating active pelagic
351 sedimentation in deeper waters prior to platform drowning. Some small normal faults (with offset
352 on the scale of tens of meters) occur in the thickest sections of MSB1 (see distal end of Line 1009,
353 Figure 4). Compared with MSB3, the reflectors of MSB1 are thinner, lower amplitude, and more
354 discontinuous (Figure 3). The parallel nature of these reflectors marks them as the result of
355 pelagic sedimentation without the influence of any significant bottom water current. A single
356 interpreted mass transport complex (MTC) occurs in the upper part of this MSB1 in the most
357 distal section of Line 1009 (Figure 4), indicating sufficient deposition up dip to result in slope
358 failure. Thick up dip deposits of MSB1 do not occur in our study area, and we conclude they must
359 have been erased by the mass wasting that occurred following the Chicxulub impact.

360 At nearby DSDP Site 95, Santonian to Campanian pelagic chinks were recovered between
361 the K/Pg boundary deposit and underlying Early Cretaceous platform carbonates (Worzel et al.,
362 1973). Up dip of the thin deposits at Site 95, it is possible that some of the pelagic sediments
363 overlying Early Cretaceous carbonates date as far back as the early Turonian, when the Yucatán
364 platform drowned (Anotine et al., 1974; Shaub, 1983; Sohl et al., 1991; Snedden and Galloway,
365 2019).

366 **4.2.2 Megasequence B2**

367 Megasequence B2 is characterized by two very high amplitude reflectors, defined here as
368 horizons H2 (bottom) and H3 (top) (Figure 3). In some places the unit is so thin that the two
369 reflectors merge into one; this is mapped as horizon H3, which represents the top of this deposit.
370 The base of this sequence is sometimes paraconformable but more often truncates underlying
371 strata. Overlying strata are conformable or sometimes onlap. Both the top and bottom of MSB2
372 represent uneven surfaces, especially along strike, and can vary vertically by >100 m over a

373 distance as short as a kilometer. MSB2 is also of uneven thickness; sometimes Horizons H1 and H2
374 are so close together they form a single reflector separating MSB1 and MSB3, and other times they
375 are separated by chaotic, often lumpy reflectors of variable amplitude. This internal chaotic unit
376 can be up to 200 m thick (as is the case in Line 1004, Figure 6; other especially thick
377 accumulations occur in Line 1006, Figure 7; and Line 1001, Figure 9) and are interpreted to
378 represent large slump deposits.

379 The K/Pg boundary deposit is well-known and easily mappable seismic reflector across the
380 entire Gulf of Mexico Basin. Originally mapped as the Mid Cretaceous Unconformity (because
381 earliest Cenozoic sediments unconformably overlie middle Cretaceous sediments; e.g., Buffler et
382 al., 1980), the discovery of the Chicxulub Crater by Hildebrand et al. (1991) cast this unit in a new
383 light. The Chicxulub impact released a massive amount of energy into the Gulf of Mexico. Seismic
384 waves led to the collapse of whole sections of the margins of the Florida and Yucatán platforms,
385 and the multiple tsunamis which followed immediately after the seismic waves led to further mass
386 wasting (e.g., Sanford et al., 2016). The K/Pg boundary deposit itself is composed of a chaotic
387 mixture of Cretaceous and older sediments jumbled together during their (re)deposition (e.g.,
388 Bralower et al., 1998). At DSDP Site 95, the K/Pg boundary unit is only about 3 m thick (Lowery
389 and Bralower, 2022), likely due to its position at the edge of the Campeche Platform. With little
390 accommodation above the Campeche Escarpment much of the material likely continued moving
391 downslope to make up the much thicker deposits in the adjacent deepwater. DSDP Sites 540 and
392 536, both deposited on paleo highs below the Campeche Escarpment, have K/Pg boundary
393 deposits around 50 m thick while deposits more than 100 m thick are evident in nearby seismic
394 data (Sanford et al., 2016).

395 With the exception of a few local slumps and depressions filled with material, the K/Pg
396 boundary deposit on the Campeche Bank is generally thin and represented by just one or two
397 reflectors. Truncation of underlying reflectors indicates that significant erosion occurred, and this
398 material must have been transported off the Campeche Bank and into the thick K/Pg boundary
399 deposits in the deep water to the east.

400 **4.2.3 Megasequence B3**

401 Megasequence B3 is primarily comprised of high amplitude parallel reflectors (Figure 3).
402 MSB3 sits conformably on top of the K/Pg boundary deposit (MSB2), with basal reflectors
403 onlapping that event layer. Some small, incised channels exist in MSB3. These channels tens of
404 meters thick and a few hundred meters wide; they erode underlying strata, are infilled by one or
405 two cross-bedded reflectors, and are overlain by flat lying reflectors that extend beyond the
406 channel. They occur rarely in MSB3, with just a handful of widely spaced channels in any one
407 profile. The largest channel we observe in MSB3 is <100 m thick and ~1 km wide (Line 1006;
408 Figure 7). Packages of chaotic, low-amplitude reflectors also occur throughout MSB3, and are
409 interpreted as mass transport complexes (MTCs) (e.g., Line 1009, Figure 4; Line 1006, Figure 7).
410 Generally, these units have a thickness on the scale of 10s of meters, often just replacing a flat,
411 high amplitude reflector with a chaotic, low amplitude reflector, but not disrupting layers above
412 and below. Rarely, they truncate underlying strata. These MTCs are laterally extensive, sometimes
413 stretching 10s of kilometers.

414 MSB3 is truncated by Horizon H4. Across much of the study area this contact appears
415 conformable, particularly in downdip areas. Up dip, truncation of underlying strata is evident,
416 although often at a fairly low angle. A major exception to this trend occurs in Line 1005 (Figure 5),
417 where extensive erosion is evident in the form of several narrow (several hundred meters wide),
418 deep (~100 m) incised channels and an erosional scarp representing ~300 m of strata truncated
419 and exposed at the paleo seafloor represented by H4. The nature of these channels is discussed in
420 Megasequence C1, below. This erosion is well-expressed on both the northern and southern ends
421 of the two strike lines we collected, where the high amplitude reflectors of MSB3 are truncated
422 (sometimes with 100s of meters of erosion) by the low amplitude reflectors of MSC1. Line 1003
423 (Figure 8) also clearly shows the high amplitude parallel reflectors of this unit and extensive
424 erosion by Horizon H4.

425 We interpret the high amplitude, roughly flat-lying reflectors of MSB3 to represent early
426 Cenozoic pelagic sedimentation in the near absence of any currents moving sediments along the
427 seafloor. Weak but erosive contourite currents are evident from the small channels that occur
428 intermittently through MSB3, but as these features are rare, it appears the seafloor was generally

429 quiescent at this time. This quiescence was brought to an abrupt end at the transition to
430 Megasequence C.

431 **4.3 Megasequence C**

432 Megasequence C (MSC) is composed of low to high amplitude, parallel, wavy, dipping, and
433 cross-bedded reflectors (Figure 3). Its lower contact with MSB is erosional (as discussed above;
434 Horizon H4) and characterized by downlapping reflectors onto the erosional surface. A second
435 erosional surface (Horizon H5) occurs partway through the unit, also characterized by
436 downlapping reflectors. This transition marks a shift from parallel reflectors with channel features
437 (MSC1) to dipping reflectors which come together on a common downlap surface (MSC2), and
438 which are truncated in the updip direction by a third erosional surface (Horizon H6) just below
439 the modern seafloor. Between this upper erosional surface and the seafloor is a thin (10s of m)
440 unit with very low amplitude reflectors (MSC3). The seafloor itself is characterized by features
441 indicative of modern contourite flow: incised moat channels and downdip drift deposits (Figure 4,
442 Figure 8). The widespread erosional surfaces that can be traced across the entire drift are
443 characteristic of contourite deposits (Faugères et al., 1999). Overall, MSC records the inception
444 and development of contourite drift deposition on the Campeche Bank, from elongated contourite
445 drifts (MSC1) to plastered drifts (MSC2) to modern moat and drift deposits (MSC3). MSC3 is mid
446 Pleistocene to Recent according to Hübscher and Nürnberg (2023), but no age control exists for
447 MSC2 or MSC1.

448 **4.3.1 Megasequence C1**

449 Throughout most of the study area, Megasequence C1 is characterized by medium to low
450 amplitude continuous reflectors downlapping on underlying units (Figure 3). In some areas,
451 particularly to the south (and best expressed in Line 1005, Figure 5), it also contains
452 discontinuous, medium to low amplitude, wavy, crossbedded reflectors, small scale amalgamated
453 channels, and very large amalgamated channels with downlapping overbank deposits. MSC1 thins
454 to the north, and is only present in the updip section of the northern profiles, and then only with a

455 maximum thickness of ~100 m. A basal erosive disconformity separates MSC1 from MSB3
456 (Horizon H4).

457 Although they are the least dramatic, the low to medium amplitude, continuous,
458 downlapping reflectors are the most common facies in MSC1. They are thickest in the updip
459 sections of Lines 1004, 1005, and 1006 (Figures 5-7). In Line 1005 they transition laterally into the
460 large, amalgamated channel deposits that make up the most striking part of MSC1 in that profile;
461 individual reflectors can be traced into channel deposits before terminating against the channel
462 wall or being truncated by another channel (Figure 5).

463 The largest of these channels are up to 400 m thick and several kilometers wide. These
464 prominent erosional features cut deep into MSB3, and the overall erosion of underlying strata is
465 on the order of hundreds of m. These channels erode updip strata and redeposit it downdip in
466 overbank deposits that pinch out toward a common downlap surface, tracking the progradation of
467 the drift deposits. Amalgamated channels along a structural high with levee deposits downdip is
468 the classic geometry of elongated contourite drifts (e.g., Rebesco et al., 2014). In Line 1005, these
469 channels start out very narrow and deep, get slightly wider and much deeper, and then get
470 progressively wider and shallower upsection (Figure 5). As this transition occurs, lateral
471 distribution of the channels widens, too. Instead of being concentrated in a narrow deep channel,
472 the bottom water current was spread out over a wider area of the ancient seafloor. This results in
473 the third seismic facies that characterizes MSC1: low to medium amplitude wavy, cross-bedded
474 reflectors and amalgamated channels.

475 Almost as striking as the geometry of these large erosional complexes is the fact that they
476 only occur at this impressive scale in a single line (1005, Figure 5). The wide line spacing in our
477 survey design allows us to characterize the overall stratigraphy of the whole drift but precludes
478 mapping interesting localized features like these channels. The only other airgun seismic survey in
479 this area (Hübscher et al. 2023) did not find any large channel features, although it had even
480 fewer lines than our own survey. This combined result of limited areal extent of large channel
481 deposits in MSC1 suggests that the strong current flow transitioned from a channel-confined
482 contourite on the southern end of the margin to a surficial drape resulting from the strong

483 deceleration of the bottom currents once they passed over this southern rampart. It is possible
484 that the facies change from MSC1 to MSC2 is the result of changing slope morphology, gradually
485 smoothing out and allowing more unimpeded flow across the whole Campeche Bank. To the
486 north, a moat channel occurs in MSC1 at the foot of the Yucatán carbonate platform in Line 1006
487 (Figure 7), but this is much smaller than the massive channels in Line 1005 (Figure 5).

488 **4.3.2 Megasequence C2**

489 Megasequence C2 (MSC2) is characterized by medium to low amplitude dipping reflectors
490 and is separated from MSC1 by a basal erosive disconformity (Horizon H5) (Figure 3). These
491 dipping reflectors can be parallel and continuous, wavy and cross bedded, or cut by small
492 channels. They thin in the downdip direction and downlap onto the basal erosive disconformity
493 separating MSC1 from MSC2. These reflectors also thin in the updip direction, where they are
494 truncated by the basal erosive disconformity of MSC3 (Horizon H6). Thick in the middle and thin
495 on the ends, MSC2 forms an overall elongated lens of sediment characteristic of a plastered
496 sediment drift (e.g., Rebesco et al., 2014). Within this lenticular deposit, a variety of facies
497 associated with contourite flow are apparent. There are small channels (10s of m deep and 100s of
498 m wide, much smaller than their larger predecessors in MSC1), wavy or hummocky cross bedding,
499 and local onlap surfaces present. These features are more common in the thicker and more steeply
500 dipping sections in Lines 1005 and 1006 (Figures 5 & 7), whereas only a few channels and wavy
501 bedding surfaces are present to the north in Line 1009 (Figure 4). Although large (100 m tall)
502 active moats associated with modern contourite flow are present on the seafloor (mapped as
503 MSC3), no channels or relict moats of similar scale are visible in MSC2. In the northern part of the
504 study area, MSC2 directly overlies the pre-drift deposits of MSB3 except in the most updip areas. It
505 is unclear whether MSC1 was originally present and then erased by subsequent erosion associated
506 with the basal disconformity of MSC2.

507 **4.3.3 Megasequence C3**

508 Megasequence C3 is a thin unit associated with the modern seafloor and a thin drape of
509 sediments separated from MSC2 by a basal erosive disconformity (Horizon H6) (Figure 3). At the

510 vertical resolution of our seismic data, it is a few reflectors thick, corresponding to 20-30 m of
511 sediment. Although the internal structure of MSC3 is difficult to resolve in our data, we can clearly
512 see the truncation of underlying strata by the basal disconformity.

513 Hübsher and Nürnberg (2023) surveyed this unit with high resolution single channel
514 parasounder data in the central and northern parts of our study area and were able to image the
515 internal structure clearly. They found sub parallel reflectors which onlap onto the underlying basal
516 disconformity; sediments are thickest in the middle and thin updip and downdip (Hübsher and
517 Nürnberg, 2023), forming a wedge of sediments that looks like MSC2 in miniature. They also
518 found sediment waves similar to those on the modern seafloor. Hübsher and Nürnberg (2023)
519 also report the results of several sediment cores taken from within this unit, the oldest of which
520 extends back to Marine Isotope Stage 11 (~400 ka). Extrapolating this sedimentation rate to the
521 basal erosive disconformity, they find an age of ~1 Ma, coincident with the Mid Pleistocene
522 Transition (MPT) (Hübsher and Nürnberg, 2023).

523 The modern seafloor is characterized by a number of features indicative of ongoing
524 contourite flow, particularly moats, which are evident in both multibeam and MCS data (Figures
525 4-6). These moats can be on the scale of 100 m, much larger than any channels observed in the
526 underlying MSC2. Moats tend to occur between 300 and 600 m water depth.

527 On the southern end of the Campeche Bank, the deeper seafloor (below ~1100 m) is characterized
528 by erosion, as a 300 m tall scarp faces directly into the oncoming current (Line 1001, Figure 9),
529 while deposition occurs across the northern end of the line. We also note the presence of a
530 narrow, ~50 m deep channel around 1300 m water depth in the saddle connecting the Yucatán
531 Strait to the top of Catoche Tongue (Figure 5-6). These down dip erosional features are much too
532 deep to be influenced by the Loop Current, which extends down only to ~ 800 m (Candela et al.,
533 2019), and we interpret them to be the result of NADW flow into and out of the Gulf of Mexico.
534 This is the depth of the southward-flowing counter current evident in the mooring observations of
535 Candela et al. (2019) (Figure 2).

536 **5. Interpretations**

537 The onset of contourite deposition occurred at the base of MSC₁, marked by a major
538 erosional event and representing the transition from parallel, continuous, high amplitude
539 reflectors to a package of medium to low amplitude reflectors characterized by a range of
540 indicators of bottom water currents (amalgamated channels, wavy, cross bedded reflectors,
541 dipping and downlapping reflectors, etc). We interpret this inception of contourite drift deposition
542 to mark the onset of the Loop Current in something like its modern form. The lack of age control
543 within these units means that we can only say for sure that the Loop Current developed sometime
544 between the K/Pg boundary and the Mid Pleistocene Transition (so, some 65 myr). By making a
545 few assumptions about the geologic context we can narrow that down significantly.

546 **5.1 Loop Current Development**

547 The stratigraphy of the Campeche Bank is characterized by Early Cretaceous carbonates
548 and then Late Cretaceous and Cenozoic pelagic sediments prior to the development of large
549 contourite deposits sometime in the Cenozoic. The lack of large scale contourite deposits below
550 MSC₁ indicates that a current with the speed and depth of the modern Loop Current did not exist
551 prior to Horizon H₄, but the occasional presence of smaller scale strike-parallel channel features
552 in MSB₃ suggests some contourite current flow across the Campeche Bank in the early Cenozoic,
553 and thus exchange of water through the Yucatán Strait at this time.

554 **Phase 1: Initiation of Contourite Deposition; Mounded Elongated Drifts**

555 The shift from pre-contourite to contourite deposits on the Campeche Bank is
556 stratigraphically sharp, with the flat-lying strata of MSB₃ incised hundreds of meters by channels
557 and other erosional features at the base of MSC₁. This erosion is most apparent at the southern
558 end of the Campeche Bank (Figure 5, Figure 9) but the basal disconformity (Horizon H₄) is
559 mappable across the entire survey area. This implies a rapid development of a strong, deep
560 current that eroded existing sediments. This event may have been less instantaneous than it
561 appears seismically, since the evidence of a ramp-up in current flow could have been erased by
562 subsequent erosion, and without age control from cores it is impossible to know how much
563 missing time is represented in the disconformity. It is also possible that a proto-Loop Current

564 existed that did not impact the seafloor across the Campeche Bank, and that the onset of
565 contourite deposition tracks the *deepening* of that current, rather than its initiation. These are
566 both questions that require sediment cores to answer properly. Regardless of how fast, exactly, the
567 transition to contourite deposition took, the base of MSC marks a major shift in the hydrography
568 of the waters overlying the Campeche Bank and in the stratigraphy of the sediments deposited
569 across it below 800 m water depth. This signals the development of a current similar in velocity
570 and depth profile to the modern Loop Current.

571 The large erosional features which characterize MSC1 in Line 1005 slowly transitioned
572 from narrow deep channels to wide, shallow channels (Figure 5). This marks either a reduction in
573 current velocity or, more likely, a gradual reshaping of the slope as erosion slowly redeposited
574 sediments to better accommodate contourite current flow.

575 **Phase 2: Transition to Plastered Drifts**

576 A more important change occurs with the transition from MSC1 to MSC2, marked by a
577 second widespread erosional disconformity (Horizon H5). Erosional disconformities mark a
578 change or break in contourite current flow, typically associated with an increase in current
579 velocity driving widespread erosion across the contourite drift (Faugères et al., 1999; Rebesco et
580 al., 2014). The erosion along this disconformity is not as dramatic as that at the base of MSC1 and
581 is primarily expressed as either truncation of underlying strata or small channel features. This
582 marks a change from elongated contourite drifts characterized by channel features and overbank
583 deposits (i.e., “elongated mounded drifts;” Rebesco et al., 2014) in MSC1 to plastered contourite
584 drifts developing along the slope without large moats up dip in MSC2. Some small moats do occur
585 in MSC2 in the northern end of the study area, but they are fairly small compared to the moats in
586 MSC3 or the modern channels in MSC1.

587 According to the contourite drift taxonomy of Faugères et al. (1999), plastered drifts can
588 occur on a slope at any depth, “where gentle relief and smooth topography favor a broad non-
589 focused bottom current” (p. 10). This seems to be the case with MSC2, where the main change is a
590 gentler slope compared to MSC1, which could facilitate the shift from mounded drift to plastered

591 drift without any reduction in current velocity. Indeed, there must have been an increase in
592 velocity to create the basal disconformity of MSC2 at Horizon H5, although this increase could
593 have been ephemeral.

594 **Phase 3: Transition back to Mounded Elongated Drifts**

595 Another abrupt change in Loop Current flow occurred at the top of MSC2, as a new
596 erosional disconformity formed (Horizon H6, which dates to the Mid Pleistocene Transition;
597 Hübscher and Nürnberg, 2023), marking the base of MSC3. This unit marks a return to contourite
598 deposition characterized by large erosional moats on the up dip end of the eastern Campeche
599 Bank. As there is no appreciable change in the slope of the Campeche Bank at this time, the
600 mechanism for this change must be an increase in current velocity.

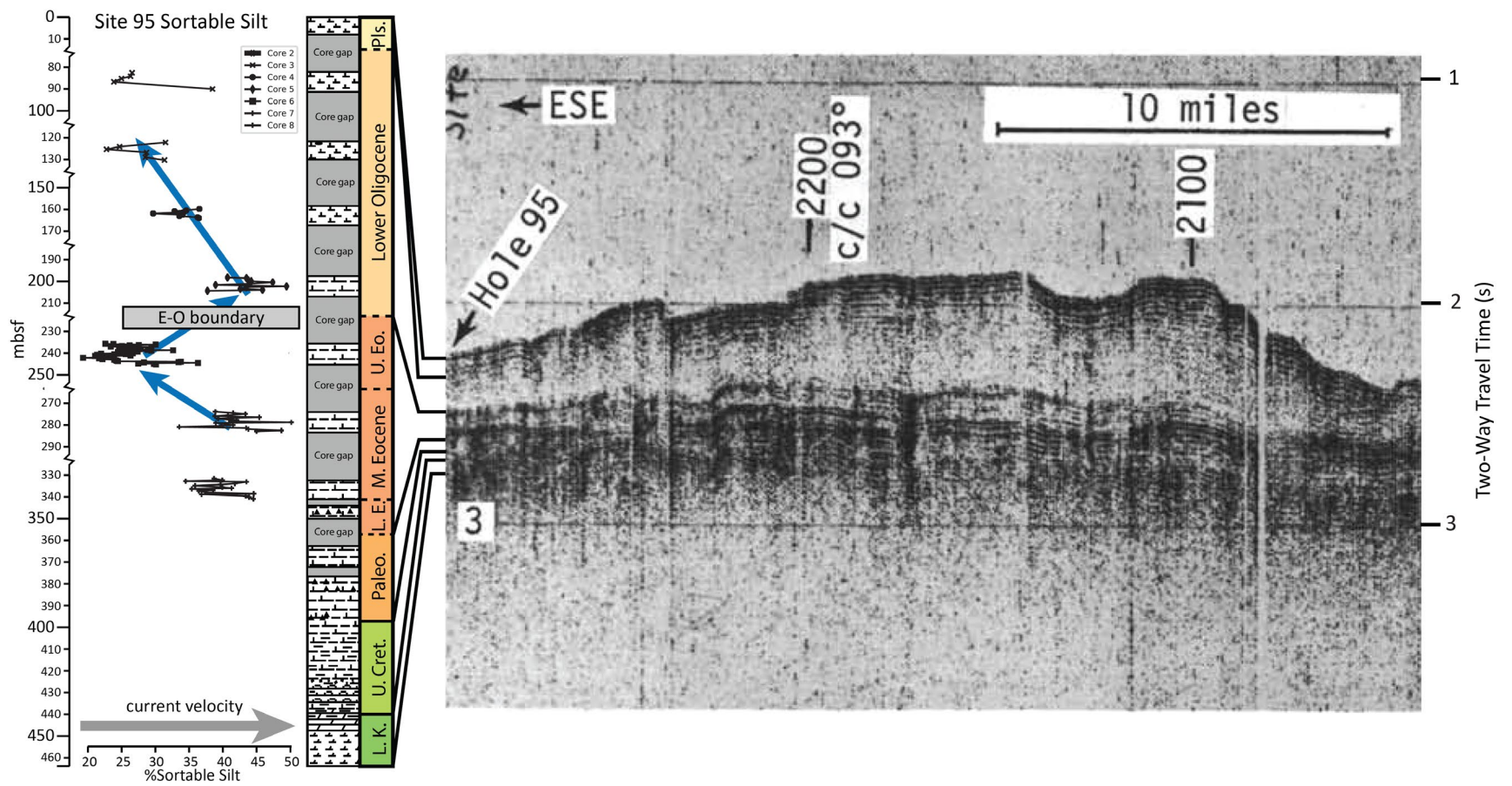
601 Hübscher and Nürnberg (2023) interpret the unit above the erosional disconformity at the
602 MPT (our H6) as evidence of weakening of the Loop Current, but, given the lack of any equivalent
603 sized moats in the underlying MSC2, we interpret the presence of moats in MSC3 as evidence of
604 strengthening of the Loop Current. Hübscher and Nürnberg (2023) based their interpretations on
605 the observation that offlapping reflectors below the MPT unconformity transition to onlapping
606 reflectors above the MPT unconformity, indicating a deeper base level of current flow interacting
607 with the seafloor below the unconformity and a shallower base level of current interaction above
608 the unconformity. However, a transition from plastered drifts below the unconformity to
609 elongated mounded drifts above, as is evident in our multichannel seismic data, indicates an
610 increase in current velocity (e.g., Rebesco et al., 2014). The presence of the unconformity itself
611 indicates that, for some period of time, current velocity increased to a point that the seafloor was
612 primarily erosive and, to be sure, the resumption of deposition above this unconformity indicates
613 a reduction in current velocity from that which caused the erosion, in agreement with Hübscher
614 and Nürnberg (2023). Core data across this transition would help determine which of these
615 hypotheses is correct.

616 **5.2 Timing of Loop Current Development**

617 No cores in or near our study area penetrate Horizon H4, which marks the base of seismic
618 facies indicative of contourite drift deposition, and so we cannot be sure of the age of this unit.
619 However, based on nearby cores and overall seismic facies we can develop a strong hypothesis.

620 DSDP Site 95 sits outside our study area on the edge of the Campeche Escarpment (Figure
621 1B). Site 95 cores show the overall stratigraphy of these deposits: a thin layer of Late Cretaceous
622 strata unconformably overlain by a thick Paleogene section, which is unconformably overlain by
623 Pleistocene ooze (Figure 10; Worzel et al, 1971). In those days, the *Glomar Challenger* would deploy
624 a streamer and airguns and conduct its own site survey prior to drilling, and according to the
625 seismic data published in the Initial Report for Leg 10 (Figure 10), at Site 95 Eocene and older high
626 amplitude reflectors are overlain by Oligocene and Pleistocene low amplitude reflectors (Worzel et
627 al., 1973). This change in seismic facies from high amplitude to low amplitude matches the shift
628 observed in our seismic profiles between MSB3 (pre-drift) and MSC (contourite drift) (e.g., Figure
629 5, Figure 8). The Leg 10 shipboard scientists noted that this change in seismic character
630 corresponds with the early Oligocene shift from chalk and cherty chalk to ooze (Worzel et al.,
631 1973). Chert is known to occur in the Eocene across the Gulf of Mexico (e.g., Buffler et al., 1982)
632 and well beyond (Muttoni and Kent, 2007). The physical characteristics (presence of chert, degree
633 of lithification) of contemporaneous sediments are unlikely to change much over such a small area
634 as the eastern Campeche Bank. We therefore think it is likely that the transition in seismic facies
635 from high amplitude reflectors in MSB to low amplitude reflectors in MSC represents the
636 sedimentological change from Eocene chalk and chert to Oligocene ooze. We thus interpret the
637 onset of Loop Current to date back to around the Eocene-Oligocene Transition (Figure 10).

638 A small increase in grainsize of sortable silt at the Eocene to Oligocene at Site 95 indicates
639 an increase in bottom water current velocity across the Eocene-Oligocene Transition (Figure 10).
640 At more than 1800 m below modern sea level this increase in current velocity is more likely driven
641 by an increase in intermediate or deep water moving into the basin than the Loop Current, but it
642 is still evidence of invigorated current flow across this major climate transition. The Eocene-
643 Oligocene Transition is associated with a strengthening of AMOC (Cramer et al., 2009; Hohbein et
644 al., 2012; Borrelli et al., 2014; Abelson and Erez, 2017; Boyle et al., 2017; Coxall et al., 2018;



645

Figure 10. Stratigraphic column of DSDP Site 95 (after Worzel et al., 1971), sortable silt from DSDP Site 95, and the original seismic profile from the Glomar Challenger with ages from the core, cropped from Worzel et al. (1971). Note discontinuous depth scale on the stratigraphic column, necessary to see detail of grain size data. Site 95 was spot cored in the Cenozoic, a common practice in the early days of DSDP. See location map in Figure 1B.

646

647 Hutchinson et al., 2019), of which the Atlantic western boundary current system, including the
648 Loop Current, is a key component.

649 Together, these observations all indicate that the Loop Current, in something like its
650 present strength, began in response to the global cooling and strengthening overturning
651 circulation at the Eocene-Oligocene Transition. This is the hypothesis we prefer because it matches
652 the timing of the change in seismic facies at the closest core to the Campeche Bank drifts.

653 Alternatively, we can extrapolate from the sedimentation rate of 3.5 cm/kyr observed in
654 the cores taken by Hübscher and Nürnberg (2019) and apply that rate to the full thickness of the
655 observed sediment drifts. This requires making some assumptions. First, we must assume that
656 sedimentation rate is constant. This is unlikely: the drifts themselves vary in thickness
657 substantially, from about 200 m to about 500 m thick. Moreover, that thickness is not evenly
658 distributed, so that MSC1 is thicker further updip than MSC2, which means that either
659 sedimentation rate or erosion varies significantly across these deposits. We must also assume that
660 the erosional disconformities don't represent much missing time. Recognizing all those caveats,
661 we find that with a sedimentation rate of 3.5 cm/kyr with no hiatuses, a 500 m thick deposit (i.e.,
662 the maximum thickness of the MSC, which presumably would minimize any hiatuses) should date
663 back to 14.3 Ma, the Middle Miocene.

664 The Middle Miocene is of course the generally accepted age for the development of the
665 Loop Current and is coeval with the onset of drift deposition in the Santaren Channel in the
666 Bahamas (12.4 Ma; Anselmetti et al., 2000) and Gardulski's (2001) estimate for the onset of drift
667 current flow across the western Florida Platform. However, this age does not match the seismic
668 facies or the chronostratigraphy of the nearest core to our study area, DSDP Site 95. The transition
669 from high amplitude reflectors to low amplitude reflectors observed at Site 95 occurs at the
670 Eocene-Oligocene Transition; within our study area it occurs at the transition from Megasequence
671 B to Megasequence C (i.e., pre-drift to drift deposits). It is certainly possible that there is a
672 significant hiatus between those two units and Pliocene or Miocene sediments are deposited on
673 top of Eocene sediments, but we do not think that is likely, especially because Miocene and
674 Pliocene sediments both appear to be entirely absent at Site 95 (Worzel et al., 1973).

675 Whatever the actual age of the base of MSC1, it seems clear that it must be older than the
676 mid Pliocene, and that the Loop Current, in something close to its current form, predates the
677 closure of the Central American Seaway and was instead initiated by some climatic shift in the mid
678 to late Cenozoic. A planned coring expedition to the Campeche Bank will answer these questions
679 more firmly.

680 **6. Conclusions**

681 Our high resolution multichannel seismic profiles of the Campeche Bank record the overall
682 evolution of sedimentation and current flow at the southern aperture of the Gulf of Mexico.
683 Megasequence A corresponds to Early Cretaceous platform carbonates. Megasequence B
684 corresponds to Late Cretaceous and early Cenozoic pelagic carbonates, bisected by the high
685 amplitude event layer associated with the Chicxulub Impact. Megasequence C corresponds to
686 contourite current deposition and records the inception and evolution of the Loop Current.
687 Megasequence C1 records the Loop Currents inception, with extensive erosion across the entire
688 Campeche Bank and seismic facies indicative of elongated mounded drift deposits. Megasequence
689 C2 records the transition to plastered drift deposits resulting from a shallowing slope as current
690 flow reshaped the sediments on the Campeche Bank, and Megasequence C3 records the transition
691 back to giant elongated mounded drift deposits in the Late Pleistocene.

692 With the exception of the short Pleistocene core in MSC3 reported by Hübscher and
693 Nürnberg (2023), the lack of cores within our study area means that we cannot say with certainty
694 when the Loop Current began. However, comparison to legacy seismic data across DSDP Site 95
695 reveals that the regional seismic facies shift from high amplitude reflectors to low amplitude
696 reflectors, which corresponds to the base of contourite deposits in our study area, dates the Loop
697 Current inception to the Eocene-Oligocene Transition. This indicates that the Loop Current
698 developed during the global reorganization of ocean circulation that accompanied the first
699 permanent southern hemisphere ice sheets. In the context of modern climate change, this is a
700 comforting observation, as it means that while a climatic tipping point for the Loop Current likely
701 exists, humanity is unlikely to cross that tipping point in any but the most extreme emissions
702 scenarios.

703 However, it should be emphasized that a comparison of seismic facies in our modern high
704 resolution seismic survey with seismic facies from low resolution (photocopied from the shipboard
705 readout; Figure 10) seismic data from 1971 is not precise, and the Loop Current may be younger
706 than the Oligocene. An alternate hypothesis, extrapolating from the sedimentation rate observed
707 by Hübscher and Nürnberg (2023) in their Pleistocene core, suggests that the base of
708 Megasequence C (and thus the Loop Current) dates to the Middle Miocene. This is in line with the
709 commonly cited age of the development of the Loop Current, based on the onset of contourite
710 drifts observed in the Florida Straits and the Santaren Channel in the Bahamas (Anselmetti et al.,
711 2000; Paulat et al., 2019) and an invigoration of current flow across the western Florida Shelf
712 (Gardulski et al., 1991). This has historically been assumed to have been driven by the closure of
713 the Central American Seaway, but more recent results suggest that the final formation of the
714 Isthmus of Panama, which blocked surface flow to the Pacific and redirected it north, did not occur
715 until the mid Pliocene (O’Dea et al., 2016). If that tectonic gateway closure did not initiate the Loop
716 Current, the most likely candidate is the climatic and oceanographic shift at the Middle Miocene
717 Climate Transition, which drove a strengthening of North Atlantic Deep Water Formation (Knutz,
718 2008; Boyle et al., 2017). The Loop Current, like downwelling NADW, is part of AMOC, and
719 increased downwelling means increased northward surface flow to compensate (e.g., Candela et
720 al., 2019). In the context of modern climate change, a Middle Miocene inception of the Loop
721 Current is particularly worrying, because we are very close to Middle Miocene $p\text{CO}_2$ values today
722 (e.g., Steinthorsdottir et al., 2021). This would imply that we are also very close to a threshold at
723 which the Loop Current could revert back to an earlier, weaker state. This reduction in the
724 northward transport of warm, salty water would weaken NADW formation and profoundly alter
725 Gulf of Mexico hydrography.

726 While we prefer an older, Oligocene age for Loop Current inception, neither hypothesis can
727 be disproven without new core material from the Campeche Bank sediment drifts. Further work
728 on this problem is imperative.

729 **Acknowledgements**

730 This work was supported by NSF-OCE-1928888, CONTEX 2018-38A, and a Pre-Drilling Activity
731 Award from the U.S. Science Support Program (NSF prime award OCE-1450528). We are grateful
732 for the patience and support of those programs and their program officers – Debbie Smith, Paloma
733 Perry, and Angela Slagle – for supporting those grants through the disruptions of a global
734 pandemic. We thank the Yucatán government for their support of this collaborative project. We
735 also gratefully acknowledge the hard work of Lee Ellett, Kolby Pedrie, Brendon Mendenhall, Nick
736 Benz, and Doug Penny in shipping, setting up, running, and troubleshooting the seismic
737 equipment, Captain David Calles-Castillo and the crew of the *R/V Justo Sierra*, Holly Smith for
738 coordinating NMFS permitting, our Protected Species Observers Yessica Vicencio, Yesenia
739 Balderas, and Elsy Olivares, and Marcy Davis for her help processing multibeam data in
740 conducting grain size analysis on DSDP Site 95 core material. We also thank Christian Hübscher
741 for discussions at early planning stages of this study, and for sharing his interesting work as it was
742 finished.

743 **Conflict of Interest Statement**

744 The authors are not aware of any affiliations or funding sources which may represent a conflict of
745 interest with this work.

746 **Data Availability Statement**

747 Large format interpreted and uninterpreted seismic profiles are presented as supplemental
748 material. Processed seismic data in SEG-Y format [will be, upon article acceptance] available from
749 the Marine Geoscience Data System’s Academic Seismic Portal [link].

750 **Figure Captions**

751 **Figure 1.** A) Regional surface currents associated with the North Atlantic western boundary
752 current, including key oceanic gateways and passages for leakage of Northern Equatorial Current
753 (N.E.C.) and Antilles Current waters into the Caribbean. B) Location map of the eastern Campeche
754 Bank and surrounding waters, showing the location of our seismic survey, DSDP Site 95, and the
755 mooring stations used to construct the vertical velocity profile reported in Candela et al. (2019)

756 (Figure 2). Basemap is the Global Multi-Resolution Topography dataset (Ryan et al., 2009) plotted
757 in GeoMapApp(www.geomapapp.org) / CC BY.

758 **Figure 2.** Southeastern Gulf of Mexico hydrography. A) Temperature (T)/Salinity (S) and
759 Temperature/Oxygen (O₂) for Yucatán Channel from Rivas et al. (2005) showing the watermasses
760 that enter the Gulf through this aperture; SUW: Subtropical Underwater; 18W: 18 Sargasso Sea
761 Water; TACW: Tropical Atlantic Central Water; AAIW: Antarctic Intermediate Water; NADW:
762 North Atlantic Deep Water. B) Generalized schematic of circulation through the Gulf of Mexico,
763 modified from Rivas et al. (2005). C) Mean current velocity in cm/s through the Yucatán Channel
764 from September 2012 to August 2016 from Candela et al. (2019). Red contours represent
765 northward flow and green contours southward counterflow; see Figure 1 for mooring locations.

766 **Figure 3.** Seismic facies, seismic units, and key horizons identified in our seismic survey. See text
767 for description of seismic megasequences and sequence sets. Figure design inspired by Boyle et al.
768 (2017).

769 **Figure 4.** Interpreted seismic profile of Line 1009, on the northern end of our study area. This
770 profile shows relatively thinner drift deposits of MSC2, while MSC1 is limited to just the most up
771 dip area, and MSC3 is not identified. A) multibeam bathymetry of active contourite moat in
772 western end of profile; B) inset interpreted seismic profile showing development of reef margins
773 in MSA (note thickening of Cretaceous pelagic sediments down dip of these margins); C)
774 interpreted seismic profile; D) line drawing of interpreted profile. MTC: Mass Transport Complex.
775 See location map in Figure 1B.

776 **Figure 5.** Interpreted seismic profile of Line 1005, which is notable for the dramatic incision of
777 MSC1 into MSB, and for the large amalgamated channels in MSC1. (see inset). A) multibeam sonar
778 bathymetry of sediment waves near western end of profile; B) inset interpreted seismic profile of
779 notable erosional features in MSC1; C) interpreted seismic profile; D) line drawing of interpreted
780 profile. See location map in Figure 1B.

781 **Figure 6.** Interpreted seismic profile of Line 1004, on the far southern end of our study area. The
782 Campeche Bank drift is narrower here and mostly limited to the far western area of this profile,

783 updip of a steep early Cretaceous reef margin. Note thick K/Pg mass transport deposit at the foot
784 of this relict escarpment. A deeper water drift complex, unrelated to the Loop Current, can be seen
785 on the eastern end of this profile. A) interpreted seismic profile; B) line drawing of interpreted
786 profile. See location map in Figure 1B.

787 **Figure 7.** Interpreted seismic profile of Line 1006, in the central part of our study area. The
788 Campeche Bank drift is thick but contains fewer channels than nearby Line 1005. A) An
789 amalgamated channel complex is present at the far updip end of MSC1; B) characteristic K/Pg
790 boundary deposit with thicker deposit with fairly thick (~100 m) build up in a paleo low; C)
791 interpreted seismic profile; D) line drawing of interpreted seismic profile. See location map in
792 Figure 1B.

793 **Figure 8.** Interpreted seismic profile of Line 1003, the updip strike line. Northward dipping
794 reflectors downlapping on Horizon H5 show deposition across the entire length of the contourite
795 drift. Extensive erosion along Horizon H4 (representing the base of contourite drift deposition) is
796 occurs across the entire profile and is particularly evident at the far northern and southern ends.
797 A) An amalgamated channel complex is present at the far updip end of MSC1; B) characteristic
798 K/Pg boundary deposit with thicker deposit with fairly thick (~100 m) build up in a paleo low; C)
799 interpreted seismic profile; D) line drawing of interpreted seismic profile. See location map in
800 Figure 1B.

801 **Figure 9.** Interpreted seismic profile of Line 1001, the downdip strike line. Of particular interest in
802 this line is the erosional escarpment on the southern end, facing the Campeche Channel. Even
803 below 1000 m there appears to be active erosion at the seafloor. A) interpreted seismic profile; B)
804 line drawing of interpreted seismic profile.

805 **Figure 10.** Stratigraphic column of DSDP Site 95 (after Worzel et al., 1971), sortable silt from
806 DSDP Site 95, and the original seismic profile from the Glomar Challenger with ages from the
807 core, cropped from Worzel et al. (1971). Note discontinuous depth scale on the stratigraphic
808 column, necessary to see detail of grain size data. Site 95 was spot cored in the Cenozoic, a
809 common practice in the early days of DSDP. See location map in Figure 1B.

810 **References**

- 811 Abelson, M., & Erez, J. (2017). The onset of modern-like Atlantic meridional overturning
812 circulation at the Eocene-Oligocene transition: Evidence, causes, and possible implications
813 for global cooling. *Geochemistry, Geophysics, Geosystems*, 18(6), 2177-2199.
- 814 Abascal, A. J., Sheinbaum, J., Candela, J., Ochoa, J., & Badan, A. (2003). Analysis of flow variability
815 in the Yucatan Channel. *Journal of Geophysical Research: Oceans*, 108(C12).
- 816 Androulidakis, Y., Kourafalou, V., Olascoaga, M. J., Beron-Vera, F. J., Le Hénaff, M., Kang, H., &
817 Ntaganou, N. (2021). Impact of Caribbean anticyclones on Loop Current variability. *Ocean*
818 *dynamics*, 71(9), 935-956.
- 819 Angstadt, D. M., Austin Jr, J. A., & Buffler, R. T. (1985). Early Late Cretaceous to Holocene seismic
820 stratigraphy and geologic history of southeastern Gulf of Mexico. *AAPG Bulletin*, 69(6),
821 977-995.
- 822 Antoine, J. W., Martin Jr, R. G., Pyle, T. G., & Bryant, W. R. (1974). Continental margins of the Gulf
823 of Mexico. In *The geology of continental margins* (pp. 683-693). Berlin, Heidelberg:
824 Springer Berlin Heidelberg.
- 825 Anselmetti, F. S., Eberli, G. P., & Ding, Z. D. (2000). From the Great Bahama Bank into the Straits
826 of Florida: a margin architecture controlled by sea-level fluctuations and ocean
827 currents. *Geological Society of America Bulletin*, 112(6), 829-844.
- 828 Arellano-Torres, E., Amezcua-Montiel, A., & Casas-Ortiz, A. (2023). The Loop Current circulation
829 over the MIS 9 to MIS 5 based on planktonic foraminifera assemblages from the Gulf of
830 Mexico. *Paleoceanography and Paleoclimatology*, e2022PA004568.
- 831 Austin Jr, J. A., Schlager, W., & Palmer, A. A. (1986). Leg 101. *Proceedings initial reports (Pt. A)*.
832 *Ocean Drilling Program, College Station, TX*.

- 833 Badan Jr, A., Candela, J., Sheinbaum, J., & Ochoa, J. (2005). Upper-layer circulation in the
834 approaches to Yucatan Channel. *Washington DC American Geophysical Union Geophysical*
835 *Monograph Series, 161*, 57-69.
- 836 Biggs, D. C. (1992). Nutrients, plankton, and productivity in a warm-core ring in the western Gulf
837 of Mexico. *Journal of Geophysical Research: Oceans, 97*(C2), 2143-2154.
- 838 Borrelli, C., Cramer, B. S., & Katz, M. E. (2014). Bipolar Atlantic deepwater circulation in the
839 middle-late Eocene: Effects of Southern Ocean gateway
840 openings. *Paleoceanography, 29*(4), 308-327.
- 841 Bosart, L. F., Bracken, W. E., Molinari, J., Velden, C. S., & Black, P. G. (2000). Environmental
842 influences on the rapid intensification of Hurricane Opal (1995) over the Gulf of
843 Mexico. *Monthly Weather Review, 128*(2), 322-352.
- 844 Boyle, P. R., Romans, B. W., Tucholke, B. E., Norris, R. D., Swift, S. A., & Sexton, P. F. (2017).
845 Cenozoic North Atlantic deep circulation history recorded in contourite drifts, offshore
846 Newfoundland, Canada. *Marine Geology, 385*, 185-203.
- 847 Bralower, T. J., Paull, C. K., & Mark Leckie, R. (1998). The Cretaceous-Tertiary boundary cocktail:
848 Chicxulub impact triggers margin collapse and extensive sediment gravity
849 flows. *Geology, 26*(4), 331-334.
- 850 Brunner, C. A. (1984). Evidence for increased volume transport of the Florida Current in the
851 Pliocene and Pleistocene. *Marine Geology, 54*(3-4), 223-235.
- 852 Buffler, R. T., J. S. Watkins, F. J. Schaub, and J. L. Worzel, 1980, Structure and early geologic
853 history of the deep central Gulf of Mexico basin, in R. H. Pilger, ed., The origin of the Gulf
854 of Mexico and the early opening of the central North Atlantic Ocean, a symposium: Baton
855 Rouge, Louisiana State University, p. 3-16.
- 856 Buffler, R.T., Schlager, W., et al. (1984), Initial reports of Deep Sea Drilling Project, v, 77, 747 p.
- 857 Burg, J.P. (1975) *Maximum entropy spectral analysis*. Stanford University

858 Candela, J., Sheinbaum, J., Ochoa, J., Badan, A., & Leben, R. (2002). The potential vorticity flux
859 through the Yucatan Channel and the Loop Current in the Gulf of Mexico. *Geophysical*
860 *Research Letters*, 29(22), 16-1.

861 Candela, J., Tanahara, S., Crepon, M., Barnier, B., & Sheinbaum, J. (2003). Yucatan Channel flow:
862 Observations versus CLIPPER ATL6 and MERCATOR PAM models. *Journal of Geophysical*
863 *Research: Oceans*, 108(C12).

864 Candela, J., Ochoa, J., Sheinbaum, J., Lopez, M., Perez-Brunius, P., Tenreiro, M., Pallàs-Sanz, E.
865 Athié, G., & Arriaza-Oliveros, L. (2019). The flow through the gulf of Mexico. *Journal of*
866 *Physical Oceanography*, 49(6), 1381-1401.

867 Chang, Y. L., & Oey, L. Y. (2012). Why does the Loop Current tend to shed more eddies in summer
868 and winter?. *Geophysical Research Letters*, 39(5).

869 Chen, C. S., 1965, The regional lithostratigraphic analysis of Paleocene and Eocene rocks of Florida:
870 Florida Geological Survey Bulletin, v. 45, 105 p.

871 Coxall, H. K., Huck, C. E., Huber, M., Lear, C. H., Legarda-Lisarrri, A., O'regan, M., Sliwinksa, K. K.,
872 Van De Flierdt, T., De Boer, A. M., Zachos, J. C., & Backman, J. (2018). Export of nutrient
873 rich Northern Component Water preceded early Oligocene Antarctic glaciation. *Nature*
874 *Geoscience*, 11(3), 190-196.

875 Cramer, B. S., Toggweiler, J. R., Wright, J. D., Katz, M. E., & Miller, K. G. (2009). Ocean
876 overturning since the Late Cretaceous: Inferences from a new benthic foraminiferal
877 isotope compilation. *Paleoceanography*, 24(4).

878 Denne, R. A., Scott, E. D., Eickhoff, D. P., Kaiser, J. S., Hill, R. J., & Spaw, J. M. (2013). Massive
879 Cretaceous-Paleogene boundary deposit, deep-water Gulf of Mexico: New evidence for
880 widespread Chicxulub-induced slope failure. *Geology*, 41(9), 983-986.

881 Denny III, W. M., Austin, J. A., & Buffler, R. T. (1994). Seismic stratigraphy and geologic history of
882 middle Cretaceous through Cenozoic rocks, southern Straits of Florida. *AAPG*
883 *bulletin*, 78(3), 461-487.

884 Droxler, A. W., Burke, K. C., Cunningham, A. D., Hine, A. C., Rosencrantz, E., Duncan, D. S.,
885 Hallock, P., & Robinson, E. (1998). Caribbean constraints on circulation between Atlantic
886 and Pacific Oceans over the past 40 million years.

887 Faugères, J. C., Stow, D. A., Imbert, P., & Viana, A. (1999). Seismic features diagnostic of contourite
888 drifts. *Marine Geology*, 162(1), 1-38.

889 Gardulski, A. F., Gowen, M. H., Milsark, A., Weiterman, S. D., Wise Jr, S. W., & Mullins, H. T.
890 (1991). Evolution of a deep-water carbonate platform: Upper Cretaceous to Pleistocene
891 sedimentary environments on the west Florida margin. *Marine Geology*, 101(1-4), 163-179.

892 Hildebrand, A. R., Penfield, G. T., Kring, D. A., Pilkington, M., Camargo Z, A., Jacobsen, S. B., &
893 Boynton, W. V. (1991). Chicxulub crater: a possible Cretaceous/Tertiary boundary impact
894 crater on the Yucatan Peninsula, Mexico. *Geology*, 19(9), 867-871.

895 Hine, A.C. (2013) Geologic History of Florida—Major Events That Formed the Sunshine State.
896 University Press of Florida, Gainesville, FL, 256 pp.

897 Hohbein, M. W., Sexton, P. F., & Cartwright, J. A. (2012). Onset of North Atlantic Deep Water
898 production coincident with inception of the Cenozoic global cooling trend. *Geology*, 40(3),
899 255-258.

900 Holbourn, A., Kuhnt, W., Kochhann, K. G., Matsuzaki, K. M., & Andersen, N. (2022). Middle
901 Miocene climate–carbon cycle dynamics: Keys for understanding future trends on a
902 warmer Earth?.

903 Hübscher, C., Dullo, C., Flögel, S., Titschack, J., & Schönfeld, J. (2010). Contourite drift evolution
904 and related coral growth in the eastern Gulf of Mexico and its gateways. *International*
905 *Journal of Earth Sciences*, 99, 191-206.

906 Hübscher, C., & Nürnberg, D. (2023). Loop Current attenuation after the Mid-Pleistocene
907 Transition contributes to Northern hemisphere cooling. *Marine Geology*, 456, 106976.

908 Hübscher, C., Häcker, T., Betzler, C., Kalvelage, C., & Weiß, B. (2023). Reading the sediment
909 archive of the Eastern Campeche Bank (southern Gulf of Mexico): from the aftermath of
910 the Chicxulub impact to Loop Current variability. *Marine Geophysical Research*, 44(2), 6.

911 Hutchinson, D. K., Coxall, H. K., O'Regan, M., Nilsson, J., Caballero, R., & de Boer, A. M. (2019).
912 Arctic closure as a trigger for Atlantic overturning at the Eocene-Oligocene
913 Transition. *Nature Communications*, 10(1), 3797.

914 Jaimes, B., & Shay, L. K. (2009). Mixed layer cooling in mesoscale oceanic eddies during
915 Hurricanes Katrina and Rita. *Monthly Weather Review*, 137(12), 4188-4207.

916 Jaimes, B., Shay, L. K., & Brewster, J. K. (2016). Observed air-sea interactions in tropical cyclone
917 Isaac over Loop Current mesoscale eddy features. *Dynamics of Atmospheres and*
918 *Oceans*, 76, 306-324.

919 Kameo, K., & Sato, T. (2000). Biogeography of Neogene calcareous nannofossils in the Caribbean
920 and the eastern equatorial Pacific—floral response to the emergence of the Isthmus of
921 Panama. *Marine Micropaleontology*, 39(1-4), 201-218.

922 Knutz, P. C. (2008). Palaeoceanographic significance of contourite drifts. *Developments in*
923 *sedimentology*, 60, 511-535.

924 Lindo-Atichati, D., Bringas, F., Goni, G., Muhling, B., Muller-Karger, F. E., & Habtes, S. (2012).
925 Varying mesoscale structures influence larval fish distribution in the northern Gulf of
926 Mexico. *Marine Ecology Progress Series*, 463, 245-257.

927 Livermore, R., Hillenbrand, C. D., Meredith, M., & Eagles, G. (2007). Drake Passage and Cenozoic
928 climate: an open and shut case?. *Geochemistry, Geophysics, Geosystems*, 8(1).

929 Lowery, C. M., & Bralower, T. J. (2022). Elevated Post K-Pg Export Productivity in the Gulf of
930 Mexico and Caribbean. *Paleoceanography and Paleoclimatology*, 37(9), e2021PA004400.

- 931 Marton, G. L., & Buffler, R. T. (1999). Jurassic–Early Cretaceous tectono-paleogeographic
932 evolution of the southeastern Gulf of Mexico basin. In *Sedimentary basins of the*
933 *world* (Vol. 4, pp. 63-91). Elsevier.
- 934 McCave, I. N., Thornalley, D. J. R., & Hall, I. R. (2017). Relation of sortable silt grain-size to deep-
935 sea current speeds: Calibration of the ‘Mud Current Meter’. *Deep Sea Research Part I:*
936 *Oceanographic Research Papers*, 127, 1-12.
- 937 Milkov, A. V., & Sassen, R. (2000). Thickness of the gas hydrate stability zone, Gulf of Mexico
938 continental slope. *Marine and petroleum Geology*, 17(9), 981-991.
- 939 Mullins, H. T., Gardulski, A. F., WISE Jr, S. W., & Applegate, J. (1987). Middle Miocene
940 oceanographic event in the eastern Gulf of Mexico: implications for seismic stratigraphic
941 succession and Loop Current/Gulf Stream circulation. *Geological Society of America*
942 *Bulletin*, 98(6), 702-713.
- 943 Mutti, M., Droxler, A. W., & Cunningham, A. D. (2005). Evolution of the Northern Nicaragua Rise
944 during the Oligocene–Miocene: drowning by environmental factors. *Sedimentary*
945 *Geology*, 175(1-4), 237-258.
- 946 Muttoni, G., & Kent, D. V. (2007). Widespread formation of cherts during the early Eocene climate
947 optimum. *Palaeogeography, Palaeoclimatology, Palaeoecology*, 253(3-4), 348-362.
- 948 National Academies of Sciences, Engineering, and Medicine. 2018. Understanding and Predicting
949 the Gulf of Mexico Loop Current: Critical Gaps and Recommendations. Washington, DC:
950 The National Academies Press. <https://doi.org/10.17226/24823>.
- 951 Nielsen, T. A. P. M., Knutz, P. C., & Kuijpers, A. (2008). Seismic expression of contourite
952 depositional systems. *Developments in Sedimentology*, 60, 301-321.
- 953 Ochoa, J., Badan, A., Sheinbaum, J., & Candela, J. (2003). CANEK: Measuring transport in the
954 Yucatan Channel. *Nonlinear Processes in Geophysical Fluid Dynamics*. Kluwer Academic
955 Publishers, Dordrecht, 275-286.

956 O'Dea, A., Lessios, H. A., Coates, A. G., Eytan, R. I., Restrepo-Moreno, S. A., Cione, A. L., Collins, L.
957 S., De Quieroz, A., Farris, D. W., Norris, R. D., Stallard, R. F., Woodburne, M. O., Aguilera,
958 O., Aubry, M.-P., Berggren, W. P., Budd, A. F., Cozzuol, M. A., Coppard, S. E., Duque-Caro,
959 H., Finnegan, S., Gasparini, G. M., Grossman, E. L., Johnson, K. G., Keigwin, L. D.,
960 Knowlton, N., Leigh, E. G., Leonard-Pingel, J. S., Vermeij, G., & Jackson, J. B. (2016).
961 Formation of the Isthmus of Panama. *Science advances*, 2(8), e1600883.

962 Paulat, M., Lüdmann, T., Betzler, C., & Eberli, G. P. (2019). Neogene palaeoceanographic changes
963 recorded in a carbonate contourite drift (Santaren Channel,
964 Bahamas). *Sedimentology*, 66(4), 1361-1385.

965 Pindell, J. L., & Kennan, L. (2009). Tectonic evolution of the Gulf of Mexico, Caribbean and
966 northern South America in the mantle reference frame: an update. *Geological Society,*
967 *London, Special Publications*, 328(1), 1-55.

968 Pinet, P. R., & Popenoe, P. (1985). A scenario of Mesozoic-Cenozoic ocean circulation over the
969 Blake Plateau and its environs. *Geological Society of America Bulletin*, 96(5), 618-626.

970 Poore, R. Z., Quinn, T. M., & Verardo, S. (2004). Century-scale movement of the Atlantic
971 Intertropical Convergence Zone linked to solar variability. *Geophysical Research*
972 *Letters*, 31(12).

973 Popenoe, P., Henry, V. J., & Idris, F. M. (1987). Gulf trough—the Atlantic
974 connection. *Geology*, 15(4), 327-332.

975 Potter, H., DiMarco, S. F., & Knap, A. H. (2019). Tropical cyclone heat potential and the rapid
976 intensification of Hurricane Harvey in the Texas Bight. *Journal of Geophysical Research:*
977 *Oceans*, 124(4), 2440-2451.

978 Rebesco, M., Hernández-Molina, F. J., Van Rooij, D., & Wåhlin, A. (2014). Contourites and
979 associated sediments controlled by deep-water circulation processes: State-of-the-art and
980 future considerations. *Marine Geology*, 352, 111-154.

- 981 Rivas, D., Badan, A., & Ochoa, J. (2005). The ventilation of the deep Gulf of Mexico. *Journal of*
982 *physical oceanography*, 35(10), 1763-1781.
- 983 Roth, J. M., Droxler, A. W., & Kameo, K. (2000). THE CARIBBEAN CARBONATE CRASH AT THE
984 MIDDLE TO LATE MIOCENE TRANSITION: LINKAGE TO THE ESTABLISHMENT OF THE
985 MODERN GLOBAL OCEAN CONVEYOR. in Leckie, R.M., Sigurdsson, H., Acton, G.D., and
986 Draper, G. (Eds.), *Proceedings of the Ocean Drilling Program, Scientific Results*, Vol. 165
- 987 Rousset, C., & Beal, L. M. (2011). On the seasonal variability of the currents in the Straits of Florida
988 and Yucatan Channel. *Journal of Geophysical Research: Oceans*, 116(C8).
- 989 Ryan, W. B. F., S.M. Carbotte, J. Coplan, S. O'Hara, A. Melkonian, R. Arko, R.A. Weissel, V. Ferrini,
990 A. Goodwillie, F. Nitsche, J. Bonczkowski, and R. Zemsky (2009), Global Multi-Resolution
991 Topography (GMRT) synthesis data set, *Geochem. Geophys. Geosyst.*, 10, Q03014,
992 doi:10.1029/2008GC002332.
- 993 Sanford, J. C., Snedden, J. W., & Gulick, S. P. (2016). The Cretaceous-Paleogene boundary deposit
994 in the Gulf of Mexico: Large-scale oceanic basin response to the Chicxulub impact. *Journal*
995 *of Geophysical Research: Solid Earth*, 121(3), 1240-1261.
- 996 Shaub, F.J. (1983). Origin of Catoche Tongue, In Bally, A.W., *A Picture and Work Atlas. Seismic*
997 *Expressions of Structural Styles*, Vol. 2 (2.2.3-129 -2.2.2-139). *American Association of*
998 *Petroleum Geologists. Studies in Geology Series # 15.*
- 999 Schmitz Jr, W. J., & McCartney, M. S. (1993). On the north Atlantic circulation. *Reviews of*
1000 *Geophysics*, 31(1), 29-49.
- 1001 Sickmann, Z. T., & Snedden, J. W. (2020). Neogene to recent evolution of the Southern Gulf of
1002 Mexico basin: Tectonic controls on deep-water sediment dispersal systems. *Basin*
1003 *Research*, 33(2), 1240-1265.
- 1004 Snedden, J. W., & Galloway, W. E. (2019). *The Gulf of Mexico sedimentary basin: Depositional*
1005 *evolution and petroleum applications*. Cambridge University Press.

1006 Sohl, N. F., Martínez, E. R., Salmerón-Ureña, P., Soto-Jaramillo, F., & Salvador, A. (1991). The Gulf
1007 of Mexico Basin. *Boulder, Colorado, Geological Society of America, Geology of North*
1008 *America*, 205-244.

1009 Steinberg, J. M., Piecuch, C. G., Hamlington, B. D., Thompson, P. R., & Coats, S. (2023). Influence
1010 of Deep-Ocean Warming on Coastal Sea-Level Trends in the Gulf of Mexico. *Authorea*
1011 *Preprints*.

1012 Steinhorsdottir, M., Coxall, H. K., De Boer, A. M., Huber, M., Barbolini, N., Bradshaw, C. D., Burls,
1013 N. J., Feakins, S. J., Gasson, E., Hendriks, J., Holbourn, A. E., Kiel, S., Kohn, M. J.,
1014 Kürschner, W. M., Lear, C. H., Liebrand, D., Lunt, D. J., Mörs, T., Pearson, P. N., Pound, M.
1015 J., Stoll, H. & Strömberg, C. A. E. (2021). The Miocene: the future of the
1016 past. *Paleoceanography and Paleoclimatology*, 36(4), e2020PA004037.

1017 Sturges, W., & Leben, R. (2000). Frequency of ring separations from the Loop Current in the Gulf
1018 of Mexico: A revised estimate. *Journal of Physical Oceanography*, 30(7), 1814-1819.

1019 Ward, W. C., Keller, G., Stinnesbeck, W., & Adatte, T. (1995). Yucatán subsurface stratigraphy:
1020 Implications and constraints for the Chicxulub impact. *Geology*, 23(10), 873-876.

1021 Weisberg, R. H., & Liu, Y. (2017). On the Loop Current penetration into the Gulf of Mexico. *Journal*
1022 *of Geophysical Research: Oceans*, 122(12), 9679-9694.

1023 Worzel, J. L., Bryant, W., and Leg 10 Shipboard Scientists (1971). *Initial Reports of the Deep Sea*
1024 *Drilling Project*, 10, U.S. Government Printing Office, Washington, DC

1025 Yilmaz, Ö. (2001). *Seismic data analysis: Processing, inversion, and interpretation of seismic data*.
1026 Society of Exploration Geophysicists.

1027

1028